Actes de la Journée MIS 2012

Roberto M'RAD, "Étude des émissions électromagnétiques conduites des convertisseurs de micro-puissance pour la téléphonie mobile".

Moisès FERBER, "Méthodologie de prise en compte a priori de la Compatibilité Électromagnétique dans l'optimisation robuste de systèmes d'électronique de puissance".

Amal EL GADDAR, "Détermination des propriétés électromagnétiques des agrégats de cellules".

Salah-Eddine ADAMI, "Optimisation de la récupération d'énergie dans les applications de rectenna (MPPT)".

Ramon DA FONSECA, "Optimisation du dimensionnement et de l'énergie pour des véhicules hybrides à pile à combustible intégrant les contraintes de durabilité".

Felicitas MENSING, "Optimisation énergétique de l'utilisation des véhicules conventionnels, électriques et hybrides. Application à l'éco-conduite".

Van hoa NGUYEN, "Contribution à une méthodologie de dimensionnement des systèmes mécatroniques : analyse structurelle et coupage à l'optimisation dynamiques".

Kai ZHANG, "Mechatronic Design under Uncertainties".

Frédéric ABRY, "Système de contrôle du vecteur de poussée d'un nanolanceur par vérin électropneumatique à l'hélium".

Ahmed MEGHNOUS, "Identification observation et commande hybride des convertisseurs de puissance".

Hao LU, "Approximation of linear infinitive dimensional systems".

Abdenour SOUALHI, "Diagnostic par utilisation de nouvelles méthodes non supervisées".

Maawad MAKDESSI, "Prognostics and Health Monitoring. Film capacitors used in Power Electronics Applications".

Ronan GERMAN, "Vieillissement calendaire des supercapacités".

Optimal dimensioning and energy management for fuel cell vehicles, integrating dynamic and durability constraints

Ramon Naiff da Fonseca

Eric Bideaux Ampère Lab; Mathias Gerard CEA; Bruno Jeaneret IFSTTAR; Matthieu Desbois CEA; Ali Sari Ampère Lab

***Abstract*— In this work, optimization methods are used in a hybrid fuel cell vehicle with two objectives: to find the best sizing of the fuel cell system and energy storage system; to define the best power split between the fuel cell system and the energy storage system. Two exact optimization methods are used (Dynamic programming and Pontryaguine maximum principle) considers the effect of the dynamics of the elements and their sub systems. The adoption of non linear control techniques on the fuel cell dynamics, allows to obtain a simple way to calculate the optimization. The durability of the fuel cell system is studied in this work such that it can be considered as a constraint to the optimization.**

***Résumé*— Dans ce travail de thèse, des méthodes d'optimisation sont utilisés pour la gestion d'énergie dans un véhicule hybride à pile à combustible. Les objectifs sont de trouver le dimensionnement optimal du système pile à combustible et de son stockage ainsi que la meilleure répartition de puissance entre le système pile à combustible et le système de stockage d'énergie. Deux méthodes d'optimisations exactes sont utilisées (programmation dynamique et principe du maximum de Pontryaguine) en considérant les effets de la dynamique des éléments et de leurs sous-systèmes. L'utilisation de techniques de commande non linéaires dans les équations dynamiques de la pile, permets de simplifier la mise en équation du système d'optimisation. La prise en compte de la durabilité de la pile à combustible est également étudiée dans ce travail. La minimisation du vieillissement de la pile est considérée comme une contrainte dans le calcul d'optimisation.**

I. INTRODUCTION

FCVs (Fuel Cell Vehicles) use fuel cells to generate electricity from hydrogen. The electricity is either used to drive the vehicle or stored in an energy storage device, such as battery pack or ultracapacitors. Since fuel cells generate electricity from electrochemical reactions, they do not burn fuel and therefore do not produce pollutants. The byproduct of a hydrogen fuel cell is water and heat.

However, there are some issues related to FCV yet. Technically, the reliability, the control of the subsystems and the energy management system represent some important improvements that should be made in this technology.

In this work, a partnership between Ampère Lab., IFSTTAR and CEA was made to deal with these technical issues and proposing scientific solutions.

The objectives of this work are focused on the FCV optimal dimensioning and the optimal energy management (which represents the optimal power split between the fuel cell system and energy storage system). Nevertheless, differently from several works done in the same domain [1,2,3], this optimization procedure must take into account the dynamic interactions between the FC subsystems and energy storage system. Another effect that the optimization should deal with is the durability, which is a novelty in this domain as well.

The remainder of this document is built up as follows: The vehicle and energy elements are presented in Section II. Section III introduces the optimization methods, the optimization problem and the results. The FC durability study is the subject of the Section IV. Conclusions and future works are given in Section V.

II. FUEL CELL VEHICLE

The reference vehicle adopted is a light vehicle of type Renault Clio. Its 60 kW ICE was replaced by a 42 kW electric asynchronous motor, that attends the requirements of the "Partnership of New Generation Vehicles" (PNGV) [4], [5].

There are several possible architectures for the FCV's. In this work, the serial architecture is adopted .In this architecture, the power demanded by the vehicle and auxiliaries is provided by the onboard fuel cell and/or onboard energy storage system. Equation 1 represents

this electric power balance, where P_{veh} is the electric power demanded by the vehicle, P_{aux} is the electric power of the vehicle auxiliaries, P_{FC} is the fuel cell power and P_{batt} is the battery power.

$$P_{veh} + P_{aux} = P_{FC} + P_{batt} \quad (1)$$

Concerning the vehicle, a simplified model, using longitudinal dynamic equations [6] and developed using the IFSTTAR modelling tool VEHLIB [7], represents the reference vehicle. This allows to obtain the efforts and consumption of the vehicle when it is submitted to a mission (road profile).

A. Fuel Cell System

The fuel cell model is based on a CEA prototype that adopts the PEMFC (polymer electrolyte membrane fuel cell) technology and has its voltage response done by the equation 2 [8]. It is used to the energy analysis and to do the analysis of the FC system dynamics.

$$V_{FC} = \beta_1 + \beta_2.T + \beta_3.T\ln(I_{FC}) + \beta_4.T\ln(P_{O_2}(St_{O_2}) - \beta_5.\frac{I_{FC}}{\beta_6}) + \cdots \quad (2)$$
$$\beta_4.T\ln(P_{O_2}(St_{O_2}) - \beta_5.\frac{I_{FC}}{\beta_6}) + \beta_7.T\ln(P_{H_2}) + \beta_8.\frac{I_L}{e^{-1268/T}} + \beta_9\ln(H_r)$$

P_x is the gas partial pressure, St is the stoichiometry, H_r is the relative humidity, T is the temperature and I_{FC} is the fuel cell current.

Equation 2 shows that the fuel cell response depends on different state variables. They are controlled by different circuits or groups. Consequently, to obtain a good response of the fuel cell, each group should control the state variable around its best operational point.

A control strategy is implemented in order to assure the nominal operational conditions of the air circuit state variables and to improve the FC dynamics. The fuel cell air circuit is usually composed sequentially from entrance to exit by the following elements: a compressor, a humidifier, the cathode volume, the humidifier and a valve to control the pressure at the cathode. The equation 3 represents the dynamic equations for the control model of the air circuit [9].

$$\begin{cases} \dfrac{d\omega_{comp}}{dt} = k_1 u_{comp} - k_2\omega_{comp} - \dfrac{k_3}{\omega_{comp}}\left[\left(\dfrac{p_{out\_comp}}{p_{atm}}\right)^{\frac{\gamma-1}{\gamma}} - 1\right]q_{comp} \\ \dfrac{dp_{out\_FC}}{dt} = k_4 q_{comp} - k_4 q_{O_2} + k_4 q_{H_2O} - k_5 p_{out\_hum} u_{vanne} \end{cases} \quad (3)$$

$$q_{comp} = f(\omega_{comp}, p_{out\_comp}) = \left(a\omega^2_{comp} + b\omega_{comp}\right)\eta\left(p_{out\_comp}\right) \quad (4)$$

$$\eta\left(p_{out\_comp}\right) = \frac{\psi_1}{\psi_2} - \frac{1}{\psi_2\left(1 - \left(\dfrac{p_{out\_comp}}{p_{atm}} - 1\right)^{\frac{\gamma-1}{\gamma}}\right)} \quad (5)$$

$$p_{out\_comp} = p_{out\_FC} + \Delta p_{humid} + \Delta p_{FC} \quad (6)$$

$$p_{out\_hum} = p_{out\_FC} - \Delta p_{humid} \quad (7)$$

Where $q_{comp}, q_{O_2}, q_{H_2O}$ are respectively the compressor air flow, oxygen flow and water flow. There is a direct relationship between the current and stoichiometry [8]. q_{O_2} and q_{H_2O} are considered as the known disturbance for the system.

Δp_{humid} and Δp_{FC} are the pressure losses in the humidifier and fuel cell respectively.

On this non linear system is applied a flatness non linear control strategy [10]. The flat outputs (Y1 and Y2) chosen are the compressor speed ω_{comp} and the pressure on downstream of the cathode p_{out_FC}. Applying the control inputs (equation 8) resulting from the flatness strategy on the simulation model, the system becomes linear and controlled in terms of pressure and stoichometry (system 9). As will be presented in section 3, the linearization is useful to the optimization task [9].

$$\begin{cases} u_{comp} = \dfrac{W_1 + \dfrac{k_3}{Y^d_1}\left[\left(\dfrac{Y^d_2 + \Delta p_{humid} + \Delta p_{FC}}{p_{atm}}\right)^{\frac{\gamma-1}{\gamma}} - 1\right] f(Y^d_1, Y^d_2) + k_2 Y^d_1}{k_1} \\ u_{vanne} = \dfrac{k_4 f(Y^d_1, Y^d_2) - k_4 q_{O_2} + k_4 q_{H_2O} - W_2}{k_5(Y^d_2 - \Delta p_{humid})} \end{cases} \quad (8)$$

$$\begin{cases} \dot{Y}_1 = W_1 = \alpha_1\left(Y^d_1 - \omega_{comp}\right) \\ \dot{Y}_2 = W_2 = \alpha_2\left(Y^d_2 - p_{out\_FC}\right) \end{cases} \quad (9)$$

B. Energy Storage System

The energy storage system adopted is composed by a pack of the Lithium-Ion batteries, more specifically the LiFePO4 technology [11].

The battery voltage V_{batt} (equation 10) depends on the temperature (T), the current (I_{batt}) and the energy (ε) in the battery. It is an empirical equation, where the relationships between the variables are obtained experimentally.

$$V_{batt} = E_{batt}(\varepsilon) - R_i(\varepsilon, T) I_{batt} \quad (10)$$

Where E_{batt} is the open circuit voltage and R_i is internal resistance.

The State of energy (SoE) of the battery, described by the equation 11, is an important variable for the battery model due to its dynamic characteristics.

$$SoE(\%) = 100.\left(\frac{\varepsilon}{\varepsilon_{\max}}\right); \quad \varepsilon = -\int P_{batt} dt \quad (11)$$

Where ε_{max} is the maximal energy supported by the battery.

III. Optimization

Exact strategies using Bellman or Pontryaguin's optimization principles were adopted by authors [3,4] for conventional hybrid vehicles. Specifically for FCV, Trichsler et al. [12] used the Pontryaguin's Maximum Principle in order to solve the optimization

problem for a heavy FCV. This optimization problem considers that the fuel cell system has a static behavior, which means that the FC dynamics was neglected in the optimization constraints. Despite this assumption, the FC has non negligible dynamics given by its subsystems dynamics (air and hydrogen feeding systems, thermal system, etc.) [13, 14], which are nonlinear in general, as presented in section 2.

This work proposes to adopt the fuel cell dynamics in the constraint of the optimization problem. The fuel cell dynamics is represented by the air circuit dynamics that is linearized by a flat nonlinear control.

The optimization problem presented in (13) has as objective to find the control input that minimizes the function J (hydrogen consumption), considering the dynamics of the system (12), constraints and boundary conditions.

$$\begin{cases} \dot{\varepsilon} = f_1(P_{batt}) = -P_{batt} \\ \dot{\omega}_{comp} = f_2(W_1) = W_1 \\ \dot{P}_{out\_FC} = f_3(W_2) = W_2 \end{cases} \quad (12)$$

$$\begin{cases} \textit{Cost Minimization}: & \textit{Constraints}: \\ J(P_{FC}^*) = min_{P_{FC}^*} \int_0^{t_f} g(P_{FC}(t))dt & P_{battmin} \le P_{batt} \le P_{battmax} \\ P_{FC}^* = argminJ(P_{FC}(t)) & P_{FCmin} \le P_{FC} \le P_{FCmax} \\ \textit{Boundary conditions}: & SoE_{min} \le SoE \le SoE_{max} \\ SoE(0) = 60\% = SoE(t_f) & \\ p_{cath}(0...t_f) = 1.2Bar & \\ St_{O_2}(0...t_f) = 1.5 & \end{cases} \quad (13)$$

The function g ($P_{FC}(t)$) in (13), represents the hydrogen consumption in g/s over a quadratic function in terms of the power delivered by the fuel cell system [20].

$$g(P_{FC}) = aP_{FC}^2 + bP_{FC} + c \quad (14)$$

In terms of the battery power:

$$g(P_{batt}) = aP_{batt}^2(t) + \beta.P_{batt}(t) + \gamma \quad (15)$$

Where $\beta = -(2a(P_{veh} + P_{aux}) + b)$ and $\gamma = \left(a(P_{veh} + P_{aux})^2 + b(P_{veh} + P_{aux}) + c\right)$.

Two exact methods were chosen to solve this optimization problem: Dynamic programming [6] and Pontryaguines maximum principle [12].

The dynamic programming (DP) method is based in a graph solution that allows to find the global optimal solution (according to the discretization). However, this method requires an important amount of memory, processing performance and needs to know the entire cycle in advance. Despite these disadvantages, the DP is useful to give a global optimum reference and to define an optimal dimensioning of the energy elements in the vehicle (FC and battery).

The Pontryaguine maximum principle can be written in a compact and symmetric form using the Hamiltonian function (16), which is the quantity that should be minimized with respect to the control inputs (equation 18).

$$H(\varepsilon, \omega, p_{cath}, P_{batt}, W_1, W_2, \lambda_1, \lambda_2, \lambda_3) = g(P_{batt}) + \lambda_1 f_1(P_{batt}) + \lambda_2 f_2(W_1) + \lambda_3 f_3(W_2) \quad (16)$$

Where λ_1, λ_2 and λ_3 are the co-states.

$$\frac{\partial H}{\partial P_{batt}} = 0 = 2aP_{batt}^*(t) + \beta(t) - \lambda_1 \Rightarrow P_{batt}^*(t) = \frac{\lambda_1 - \beta(t)}{2a} \quad (18)$$

$$\frac{\partial H}{\partial W_1} = 0 = \lambda_2; \frac{\partial H}{\partial W_2} = 0 = \lambda_3$$

These results show that the optimization problem depends only on the co-state λ_1 and the power demanded by the vehicle and auxiliaries. Therefore, thanks to the non linear control applied to the FC dynamics, it is possible to minimize the Hamiltonian explicitly.

The choice of λ_1 is made using the bisection method over a λ_1 acceptable domain up to obtain the boundary condition.

Another approach, based in the Pontryaguine principle as well, is being developed such that it can give a local optimization close to the global optimization without knowing the entire cycle in advance (information of λ_1). The figure 1 presents the block structure of this strategy. More details about this solution can not be presented yet due to a pattent procedure.

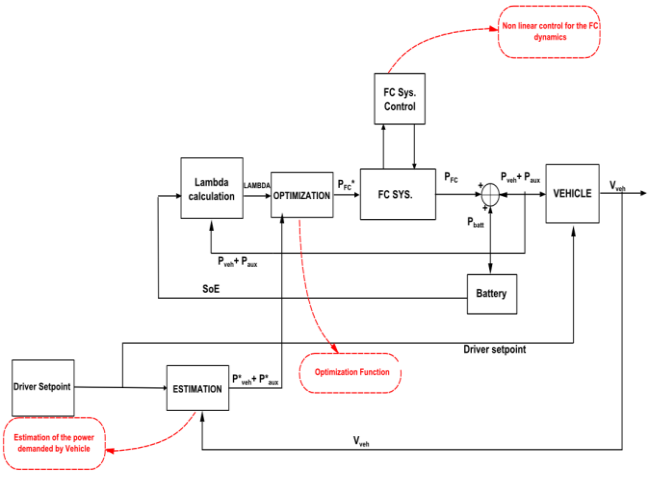

Fig1. Control block for the updated optimization strategy

A. Optimal Dimensioning

The dynamic programming (DP) is applied to find the optimal dimensioning of the fuel cell system and

battery. The procedure applies the DP for each configuration and verifies the response in terms of hydrogen consumption. In this procedure, when the system increases, the mass and the equivalent hydrogen consumption increase, modifying the optimization procedure. The response of the dimensioning is linked to the type of the drive cycle imposed to the vehicle. The figure 2 shows the response for a New European Drive Cycle (NEDC) [15]. The best hydrogen consumption for this cycle is obtained with 3kWh for the battery and 25kW for FC maximal power. This is explained by the braking recovering potential of the battery and the best operational points for the fuel cell in terms of the consumption and mass.

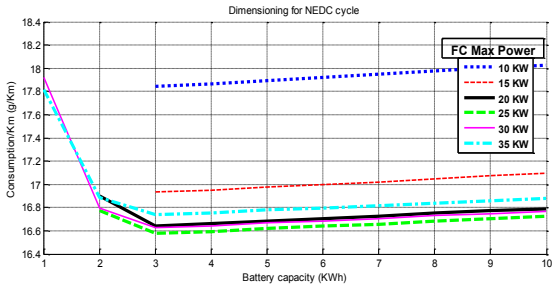

Fig2. Optimal Dimensioning

B. Optimal Energy Management

The NEDC is imposed to the reference vehicle and the results in terms of the power split optimization are presented in Fig. 3 and Fig. 4.

Figure 3 shows that the battery is responsible for the dynamic response while the fuel cell system delivers an almost constant power. This represents a typical behavior of a hybrid series architecture, where the vehicle dynamics is decoupled from the fuel cell system dynamics, which operates in optimal conditions. Therefore, about 181 g of hydrogen (representing 16.4 g/km) are necessary to execute the cycle function of the constraints and boundary conditions assigned in the optimization problem, such as the SoE condition (Fig. 4).

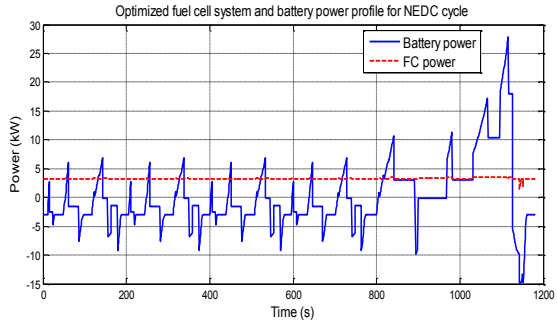

Fig 3 . FC and Battery power response

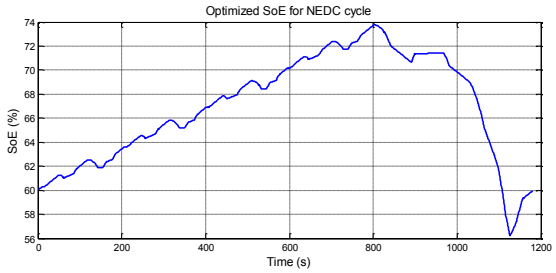

Fig 4. SoE response

IV. Degradation Study

The performance of a PEM fuel cell or stack is affected by many internal and external factors [16]. Performance degradation is unavoidable, but the degradation rate can be minimized through an optimization of the FC operation that considers the degradation as a constraint. The degradation constraint is a dynamic function (equation 14) where each important effect is represented by an operational mode, such as [17]:

1 – Stop\Start procedure: $f_1(P_{FC})$

2 – Idling condition operation: $f_2(P_{FC})$

3 – Load changing operation: $f_3(P_{FC})$

4 – High power load operation: $f_4(P_{FC})$

$$\dot{x} = \sigma_1 f_1(P_{FC}) + \sigma_2 f_2(P_{FC}) + \sigma_3 f_3(P_{FC}) + \sigma_4 f_4(P_{FC}) \qquad (14)$$

For this study, it is necessary to determine the degradation rates σ_i related to the operational modes. The continuation of this work intends to solve the optimization problem considering the degradation dynamics (equation 14).

V. Conclusions and Future Works

Exact optimization methods were implemented with the objective to define the optimal sizing and the optimal energy management in a fuel cell vehicle. Using the dynamics of the elements as constraints, the optimization problem is solved in an explicit way thanks to the control strategy applied for the fuel cell dynamics. However, the solutions provided so far, are dependent to the knowledge of the entire cycle. As a future work, an approach that overcomes this drawback is being developed at the moment. Another future development is the implementation of the fuel cell durability in the optimization problem as a constraint.

References

[1] L.M. Fernandez, P. Garcia, C.A. Garcia, and F. Jurado, “Hybrid electric system based on fuel cell and battery and integrating a single dc/dc converter for a tramway”,Energy Conversion and Management, vol. 52, pp. 2183-2192, 2012.

[2] Y.Zhu, Y. Chen, Z. Wu and A. Wang, "Optimization design of an energy management strategy for hybrid vehicles", Int. J. Alternative Propulsion, vol. 1, p. 47:62. 2006

[3] M. Koot, J.T.B.A. Kessels, B. de Jager, W.P.M.H.Heemels, P.P.J. van den Bosh and Steinbuch, "Energy Management Strategies for Vehicular Electric Power Systems", IEEE transactions on vehicular technology, vol. 54, pp. 771-782, 2005.

[4] T. C. Moore and A. B. Lovins, "Vehicle design strategies to meet and exceed pngv goals," SAE, 2000.

[5] X. Wu, B. Cao, X. Li, J. Xu, and X. Ren, "Component sizing optimization of plug-in hybrid electric vehicles," Applied Energy, 2010.

[6] E. Vinot, R. Trigui, and B. Jeanneret, "Optimal management of electric vehicles with hybrid storage system," in Proc. IEEE VPPC- Vehicle power and propulsion conference, Lile, France., pp. 1 – 6, 2010.

[7] R. Trigui, F. Badin, and B. Jeanneret, "Modélisation systémique de véhicules hybrides en vue de la prediction de leurs performances énergétiques et dynamiques- construction de la bibliothéque de modéles vehlib," Recherche Transports Sécurité, pp. 129–150, 2004.

[8] Jean Philippe Poirot-Crouvezier, Modelisation dynamique des phenomenes hydrauliques, thermiques et electriques dans un groupe electrogene à pile à combustible destiné à l'application automobile. Phd thesis, Institut National Polytechnique de Grenoble, 2000.

[9] Ramon da Fonseca, Eric Bideaux, Bruno Jeaneret, Mathias Gerard, Mathieu Desbois and Ali Sari, "Energy management strategy for fuel cell vehicle", In Proc. 12th International Conference on control, Automation and Systems. 2012

[10] M. Fliess, J. Levine and P. Rouchon, "Flatness and defect of nonlinear systems: introductory theory and exemples", International Journal of Control, 1995, Vol. 61, 1327-1361

[11] M. Montaru and S. Pelissier, "Frequency and temporal identification of a li-ion polymer battery model using fractional impedance," In Proc. Les Rencontres Scientifiques de l'IFP - Advances in Hybrid Powertrains, vol. 65, pp. 67–78, 2008.

[12] P.J. Thritschler, S. Bacha, E. Rullière and G. Husson, "Energy management strategies for an embedded fuel cell system on agricultural vehicles", ICEM 2010. 19th International Conference Electrical Machines, Rome, Italy, pp. 1-6, 2010.

[13] A. Vahidi, A. Stefanopoulou, and H. Peng, "Current management in a hybrid fuel cell power system: A model predictive control approach," IEEE Transactions on control systems technology, vol. 14, pp. 1047–1057, 2006.

[14] J. T. Pukrushpan, A. Stefanopoulou, and H. Peng, "Modeling and control for pem fuel cell stack system," In Proc. American Control Conference, vol. 4, pp. 3117 – 3122, 2002.

[15] Ramon da Fonseca, Eric Bideaux, Mathias Gerard, Matthieu Desbois and Bruno Jeaneret, "Hybrid Electric System for an Hydrogen Fuel Cell vehicle and its Energy Management", SAE World conference and Exibition, 2012.

[16] J. Wu, X.Z.Yuan, J.J. Martin, H. Wang, J. Zhang, J. Shen, S. Wu and W. Merida, "A review of PEM fuel cell durability: Degradation mechanisms and mitigating strategies", Jornal of power sources, Vol. 184, 104-119, 2008.

[17] Pucheng Pei, Qianfeng Chang and Tian Tang, "A quick evaluating method for automotive fuel cell lifetime", International Journal of Hydrogen Energy, Vol.33, 3829-3836, 2008.

Assessment of 0.5 T static field exposure effect on yeast and HEK cells using electrorotation

A. El Gaddar, M. Frenea-Robin, D. Voyer, N. Haddour, L. Krahenbuhl

***Abstract*— The present study aims to examine the influence of a static magnetic field (SMF) on Human Embryonic Kidney 293 cell morphology, growth and physiology. This last property is investigated by comparing the electrorotation spectrum of the cells exposed for 72 h to a 0.5 T uniform SMF with that of unexposed cells. We compare also the proliferation kinetics for each case and their morphology was examined by scanning electron microscopy (SEM). The results show a slight effect of SMF on cell physiology and no effect on cell growth and morphology.**

***Résumé*— Dans cette étude on s'intéresse à examiner l'influence du champ magnétique statique (SMF) sur la morphologie, croissance et la physiologie des cellules HEK 293. Cette dernière propriété est examinée en comparant le spectre d'électrorotation des cellules exposées pendant 72 h à un champ magnétique statique de 0.5 T avec celui de cellules non exposées. Nous comparons aussi la cinétique de prolifération pour chaque cas et leur morphologie a été examinée en utilisant la microscopie électronique à balayage (SEM). Les résultats montrent un effet léger du champ magnétique statique sur la physiologie cellulaire et aucun effet sur la croissance cellulaire et la morphologie.**

I. INTRODUCTION

In the past few years, new magnetic microdevices have been designed for the development of new biological and biomedical applications, such as cell separation, cell levitation [1][2], and cell trapping. With the recent advances in the development of high performance micromagnet arrays, magnetic flux densities as high as 1 T and very high field gradients can now be generated at the micrometer scale [3][4]. *In-vitro* studies reported in the literature usually evaluate biological effects of SMFs by monitoring cell growth, morphology, apoptosis, genotoxicity, orientation, metabolic activity or gene expression. Zhou and coworkers also proposed to use electrorotation to assess potential effects on yeast cells exposed to 50 Hz, 8 and 80 µT fields for 4h or less. While no effects were reported in this case, the technique is particularly appropriate to detect potential changes induced in cell membrane physiology, as those would modify the anti-field rotation peak observable on the ROT spectrum. Indeed, electrorotation (ROT) has also been extensively used to monitor the physiological state of cells as well as the evolution of cell dielectric properties in response to various stimuli, such as a temperature rise or a chemical treatment[5]. To our knowledge, since the study performed by Zhou and coworkers, no comparable assessment of magnetic field effects using electrorotation has been reported.

In this paper, we propose to analyze the effects of a 0.5 T uniform SMF on Human Embryonic Kidney (HEK 293) cells. The cell growth and viability have been studied using the trypan blue exclusion. The potential changes in the morphology have also been tracked from ROT experiments.

II. MATERIALS & METHODS

A. Cell Culture

HEK 293 cells were obtained from Health Protection Agency Culture Collections, Salisbury UK. The cell lines were grown at 37°C under 5% CO2 in Dulbecco's Modified Eagle Medium high glucose (DMEM) supplemented with 10% fetal calf serum, 100 µg/ml streptomycine and 100 U/ml penicillin. Cells were passaged two times weekly in order to maintain them in the exponential growth. However, the medium of culture is highly conductor; before electrorotation manipulation, cells have to been transferred in a low conductor medium (≈ 50 mS/m).

B. Magnetic Field Exposure

The exposure source consisted of a Halbach cylinder (Magnetic Solutions), which is a hollow permanent magnet cylinder producing a uniform 0.5 T magnetic field inside the bore Figure 1. It features inner and outer diameters of 54 mm and 140 mm cm respectively and is 60 mm in height. To investigate the effects of 0.5 T Static magnetic fields on human cells HEK 293, a Petri dish with cells was put in the middle of magnet cylinder for 72 hours, while another one (control dish) was kept in the same incubator, far away from the magnetic source.

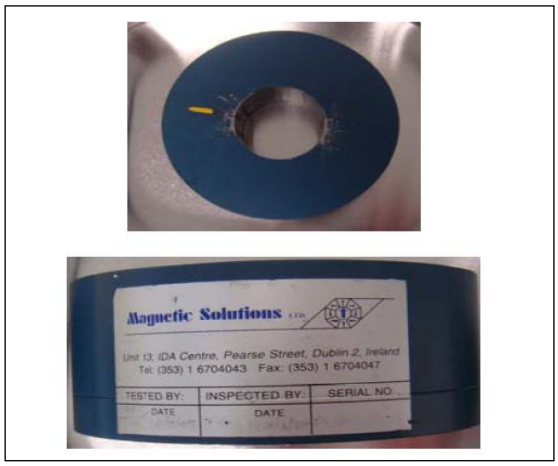

Fig.1. Top and side views of the Halbach cylinder

III. ROT MEASUREMENT

A. *Microsystem*

The using microsystem is constituted by four polynomial electrodes, coated with thin layer of gold (100 nm) and separated by (400 nm). This shape for the electrodes has been chosen because it produces a uniform electric field in the inter electrode space where the cells are placed.

B. *Data Acquisition and Image Processing*

rotating electrical field was generated by applying four sine waves in phase quadrature to a quadrupole electrode system for frequencies ranging between 10 kHz and 80 MHZ. For each frequency point, a video sequence is acquired using the Zeiss Axiovision software. Cell rotation speed was obtained from the acquired image sequences using the Matlab® Image Processing Toolbox.

C. *Scanning Electron Microscopy (SEM)*

The SEM is a microscope that uses the backscattered electrons to form images. This microscope consists of an electron gun and an electronic column which produce a fine electronic probe on the sample, sample holder allowing to move the sample in three directions and detectors (Robinson) allowing to get and to analyze the radiations emitted by the sample. The used SEM is characterized by a high resolution 2nm when electrons moved across an electric potential difference of 30 KV at a working distance of 5 mm.

IV. RESULTS

A. *ROT Spectrum*

The technique of electrorotation allows to determine the dielectric properties (capacitance and conductance) of cells [6], that depend on the composition of cell membrane and cytoplasm. Thus any cells physiology modification will undoubtly lead to a ROT spectrum modification. To evaluate the effect of the 0.5 T SMF on the cell physiology, the ROT spectra of exposed and not exposed cells were compared Figure.2 for 12 to 14 individual cells stemming from different experiences.

It can be noticed that the spectra of unexposed HEK cells have nearly the same appearance than that found in the literature [7]. The Figure does not show a major change in the spectrum before and after exposure to 0.5 T of SMF. This result tends to indicate that the physiology of the cell membrane and cytoplasm was not affected by the SMF. However, cells that have undergone the SMF rotate more quickly than the unexposed ones but the difference still remains low and above all the frequency of the field peak is not modified.

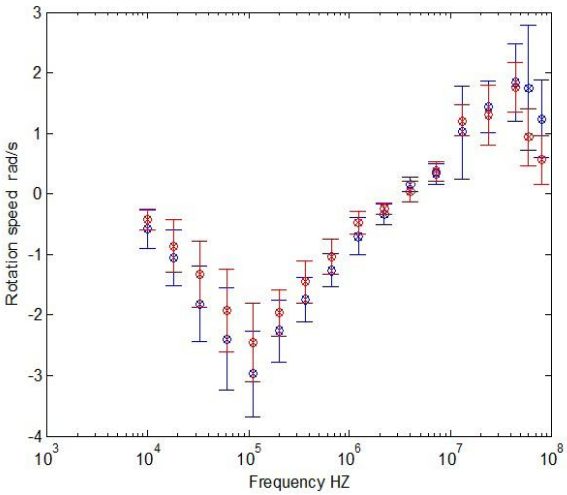

Fig.2. Comparison of ROT spectra for exposed(blue) and unexposed cells(red).

B. *Cell proliferation*

The proliferation kinetics was realize by using trypan blue exclusion method to calculate the viable cells for both the exposed and control samples Figure.3. The experiment was repeated three times to ensure the reproducibility of the results. After 24 hours we observes that control cultures have a slightly greater viability than the ones subjected to the 0.5 T magnetic field, after 48 hours The growth is almost identical for both cases and after 72 hours the cultures undergone the SMF proliferation is a little more important than control culture. But it still remains insignifically regarding error bars.

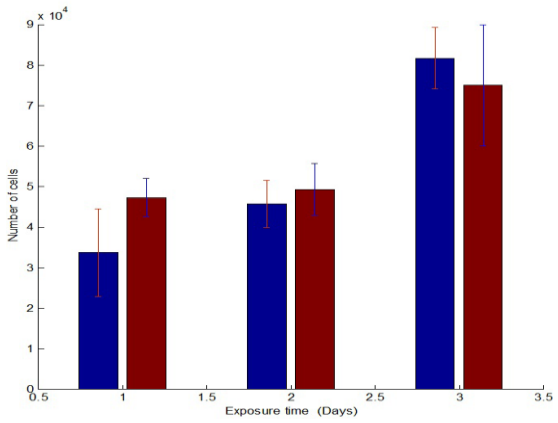

Fig.3. Comparison of cell proliferation after 24, 48,72 hours of incubation, between exposed cells(blue) and unexposed(red)

C. Scanning Electron Microscopy-Cell Morphology

The evolution of the cell morphology has been observed at different moments of the culture process for the exposed and unexposed cells. The pictures taken after 24h, 48h and 72h Figure.4 shows that there is no change in cell morphology.

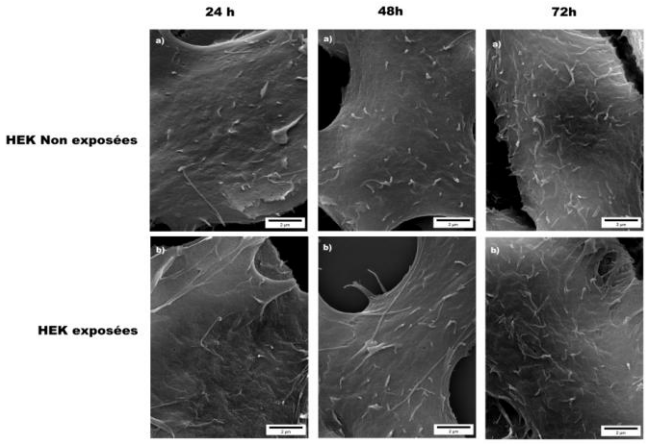

Fig.4. Comparison of SEM photographs after 24h, 48h, 72h of incubation for unexposed and exposed HEK293 cells

V. CONCLUSION

In this study we used two methods to evaluate the effect of 0.5 T SMF on HEK293 cells; the first was electrorotation, this technique allowed us to conclude that SMF has no effect on the membrane physiology. The second was the trypan blue exclusion; it shows that cell viability and mortality are not affected by SMF. We also observed that SMF had no effect on HEK cells morphology. As a perspective, we plan to use impedance measurement method by cell concentration utilizing negative dielectrophoresis to determine electric characteristic of the cells aggregates.

REFERENCES

[1] Xia N, Hunt TP, Mayers BT, Alsberg E, Whitesides GM, Westervelt RM, · Ingber DE. 2006. Combined microfluidic-micromagnetic separation of living cells in continuous flow. Biomedical Microdevices 8: 299-308.

[2] Winkleman A, Gudiksen KL, Ryan D, Whitesides GM, Greenfield D, Prentiss M. 2004. A magnetic trap for living cells suspended in a paramagnetic buffer. Applied physics letters 85(12) : 2411-2413.

[3] Dumas-Bouchiat F, Zanini LF, Kustov M, Dempsey NM, Grechishkin R, Hasselbach K, Orlianges JC, Champeaux C, Catherinot A, Givord D. 2010. Thermomagnetically patterned micromagnets. Applied Physics Letters 96 : 102511

[4] Pivetal J, Osman O, Vezy C, Frénéa-Robin M, Dumas-Bouchiat F, Dempsey NM, Givord D, Simonet P, Buret F, Reyne G, Haddour N. 2010. Trapping of Magnetically-Labelled Liposomes on Flat Micro-Patterned Hard Magnetic Films. AIP Conference Proceedings.1311: 192-197.

[5] Zhou X-F, Burt JPH, Pethig R. 1998. Automatic cell electrorotation measurements: studies of the biological effects of low-frequency magnetic fields and of heat shock. Phys. Med. Biol. 43: 1075–1090.

[6] Pushkar P. Lele, Manish Mittal, and Eric M. Furst. Anomalous Particle Rotation and Resulting Microstructure of Colloids in AC Electric Fields.American Chemical Society 2008.

[7] D. Zimmerman, M.Kiesel, U.Terpitz, A.Zhou, R.Reuss, J.Kraus, W.A. Schenk, E.Bamberg, V.L. Sukhorukov. A Combined Patch-Clamp and Electrorotation Study of the Voltage- and Frequency-Dependent Membrane Capacitance Caused by Structurally Dissimilar Lipophilic Anions . Springer Science 2008.

Electrochemical Double Layer Capacitors (supercapacitors) ageing studies in the particular context of personal ground transports

Ronan German, ***Laboratoire Ampère UMR CNRS 5005, Université Lyon1***
Pascal Venet, *Laboratoire Ampère UMR CNRS 5005, Université Lyon1*
Ali Sari, *Laboratoire Ampère UMR CNRS 5005, Université Lyon1*
Jean-Michel Vinassa, IMS UMR CNRS 5218,Université Bordeaux 1
Olivier Briat, IMS UMR CNRS 5218, Université Bordeaux 1

***Abstract*—This documents is a summary of the 2 first PHD years of Ronan German. Reserches are supervised by Pascal Venet and Ali Sari. The main goal of PHD is to integrate ageing constraints effects of personal ground transports on existing ageing laws concerning electrochemical double layer capacitors (EDLC). Firstly a quick introduction will present the PHD problematic. Secondly the different accomplished works will be introduced (test benches conception, EDLC impedance modeling, experimental ageing results interpretation). Finally conclusion and perspectives will present the envisaged future researches.**

***Résumé*—Ce document est un résumé des travaux de thèse effectués par Ronan German durant les deux premières années. Les recherches sont encadrées par Pascal Venet et Ali Sari. Le but principal du doctorat est d'intégrer aux lois de vieillissement préexistantes, l'effet des contraintes de vieillissement rencontrées par les supercondensateurs, dans l'environnement des transports routiers (vehicules mild hybrid ou full hybrid) . La problematique et l'objet d'étude (le vieillissement des supercondensateurs) seront tout d'abord présentés. Dans un second temps les travaux accomplis seront montrés (construction des bancs d'essais, modélisation d'impedance, interprétation des résultats de vieillissement). Enfin viendront conclusions et perspectives.**

I. INTRODUCTION

A. EDLC ageing

Supercapacitors (SC) also called electrochemical double layer capacitors (EDLC) are energy storage systems. EDLC storage principle is based on the double layer effect as shown on Fig. 1. Double layer effect is an ionic/ electronic electrostatic storage. It occurs when a potential difference (ΔV) appears between electrically supplied electrode and an electrolytic solution. As there is no faradic storage as in batteries, they are particularly interesting thanks to their high cyclability and their high power density. Nevertheless their mass energy is lower than batteries. They can be used in transports domain such as trolleybuses or in railway transports in applications where peak power is needed (braking energy recovery or stop and start systems). In transports area reliability and diagnostic of energy storage systems (ESS) are major issues. As a matter of fact as any ESS, EDLC are subject to ageing. Fig. 1 represents ageing causes and effects of EDLC. EDLC electrodes are porous to maximize contact surface between electrode and electrolyte. To get porous structure from carbon some chemical treatments are necessary. These treatments let parasitic surface groups on electrodes which react by redox reactions under voltage and temperature constraints of EDLC. The solid reaction products start to block electrode porosity causing capacitance loss. Produced off-gas makes electrode cracks. Binding agent ageing causes electrode grain drops implying an equivalent serial resistance (ESR) increase. Thus EDLC Ageing has an impact on EDLC impedance. That's why impedance will be used for EDLC state of health monitoring in our project.

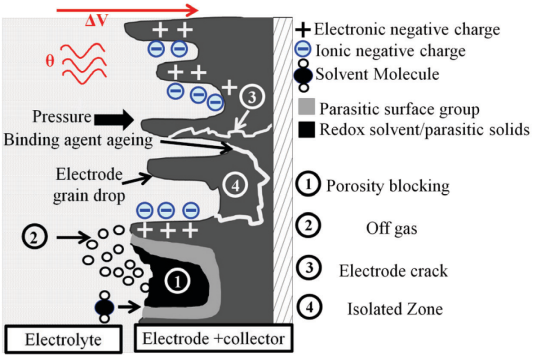

Figure 1. Ageing causes and effects of EDLC

B. *Problematic*

The major acceleration factors on EDLC ageing are temperature, voltage and current. Some studies have already been achieved on floating ageing (constant temperature and voltage constraints) and on cycling ageing (high current profiles). Nevertheless the environment of personal ground transports implies complex ageing constraints as shown on Fig. 2. As a matter of fact they are subject to parking phases which are equivalent to floating ageing and active driving phases which are equivalent to cycling ageing (high current). Moreover the presence of DC-DC converters on transports electrical network is a possible source of ageing. Finally the impact of day and night temperature changes has to be verified. The main goal of my PHD is to find ageing laws for EDLC taking into account all parameters of ground transports domain.

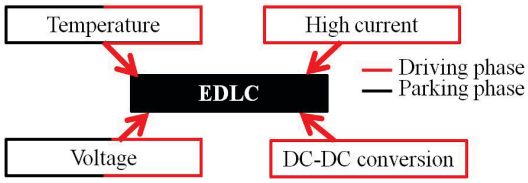

Figure 2. Ageing constraints on EDLC in personal ground transports

II. Works and Methods

A. *Works accomplished*

The works on my thesis are divided in four parts:

- Building experimental test bench for EDLC ageing and characterization
- Writing experimental protocols
- EDLC impedance model comparison
- Experimental EDLC ageing results

B. *Building experimental test bench*

Fig. 3 presents the experimental platform used for obtaining experimental results presented in this article.

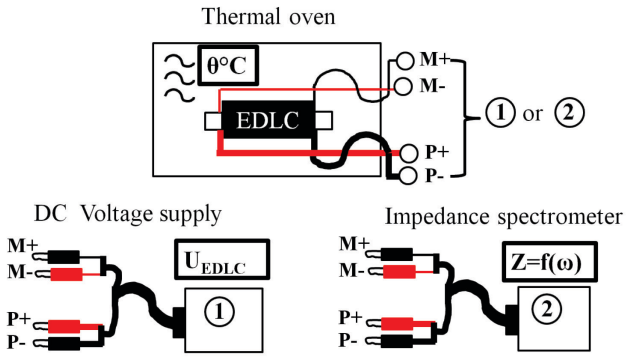

Figure 3. Presentation of experimental platform

It has been shown (Part. I.B) that ageing speed mainly depends on temperature and voltage constraints. EDLC is placed in a programmable precision incubator for applying the temperature constraint. As EDLC needs to be kept at the same voltage (we are currently studying floating ageing) a dispositive of electrical connection is plugged on EDLC. To not disturb EDLC temperature (as a matter of fact EDLC impedance is dependant of temperature) this connection dispositive is placed outside incubator thanks to a thermo isolated hole. As impedance of EDLC is the same order of magnitude than the electrical wires (0.1mΩ) a 4 point dispositive must be connected (M+ and M- are the pins used for voltage measurement and P+ and P- are the power pins where the charging /discharging current goes through). These pins are connected during ageing time to a DC voltage supply and regularly replaced by an impedance spectrometer for achieving characterizations.

C. *EDLC impedance model comparison[1]*

1) *Single pore model*

Single pore model has been developed for modeling frequency behavior of a porous structure of EDLC uniquely composed of perfectly identical cylindrical pores. In this working hypothesis, porous structure impedance can be modeled using simple equivalent components as shown in figure 4 .

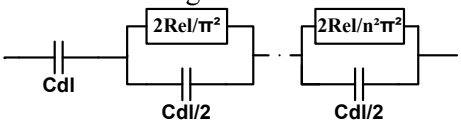

Figure 4 Equivalent electrical circuit of porous structure for single pore sized

C_{dl} represents the LF (low frequency) double layer capacitive effect; this parameter is called porous structure capacitance. R_{el} is called electrolytic resistance. Parallelized R_{el} and C_{dl} equivalent circuits model the increasing difficulty for charges to penetrate deep in the pore with increasing electrical signal frequency. Impedance of electrode can be defined by the following expression [2]:

$$Z_{PorousStructure} = \sqrt{\frac{R_{el}}{j\omega C_{dl}}} \times \coth\left(\sqrt{j\omega C_{dl} R_{el}}\right) \quad (1)$$

Experimental results show that real EDLC porous

impedance behavior appears to be far away from a single pore sized porous electrode model. It has been interpreted by Song and al [3] as the result of a pore size distribution on real porous electrode. This implies slow diffusion and sluggish surface reconstruction between the different pore sizes. Time constants of these phenomena can go from one second up to several hours. Thus influence of pore distribution on porous impedance occurs in the LF range (10 mHz to 100 mHz).

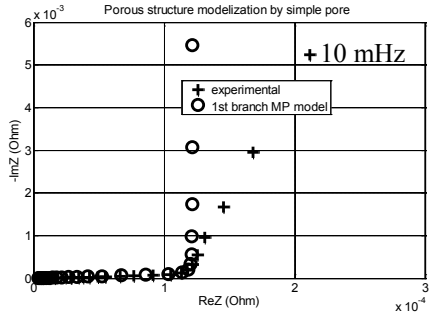

Figure 5 Comparison between EDLC electrode impedance and single pore model Nyquist diagrams

2) CPE Model

As the single pore model was precise to model HF diffusion phenomena Kötz and al. in [4] proposed to combine strength of single pore with CPE component including CPE element into the single pore equation (Eq.1). They replaced consequently the frequency dependant factor $j\omega C_{dl}$ by $(j\omega)^{1-\gamma} C_{dl}$ in Eq. 1 to model pore distribution influence in LF. This model is called the CPE model. Then mathematical expression of porous structure impedance becomes [4]:

$$Z_{PourousStructure} = \sqrt{\frac{R_{el}}{(j\omega)^{1-\gamma} C_{dl}}} \times \coth(\sqrt{(j\omega)^{1-\gamma} C_{dl} R_{el}}) \qquad (4)$$

Equivalent electronic circuit is obtained by replacing the serial C_{dl} capacitance by a CPE element (C_{dl}, γ) in figure 4 to model LF impedance. As the HF diffusion phenomena were correctly modeled in single pore model the HF part of the circuit does not change.

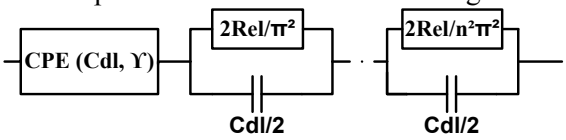

Figure 8. CPE model equivalent circuit [4]

The figure 9 presents the graphs of experimental porous structure impedance and the CPE model fitting.

LF distribution associated phenomena effects appear to be well represented by the CPE model. The gain in term of LF fitting precision is important compared to single pore model. Moreover the simple mathematical expression makes it easy to extract parameters with a simple fitting algorithm. Nevertheless, two major drawbacks appear. The first one is the fact that CPE element is a fractional derivative element. It cannot be represented by an equivalent LRC circuit. The second one concerns the health monitoring of EDLC. Indeed, evolution of global parameters such as (C_{dl}, γ, R_{el}) does not allow to know if there is some pore category which are more or less concerned by the ageing processes. Identification of separated pore impedance evolution could enable to monitor the effect of different chemical ageing reactions [7].

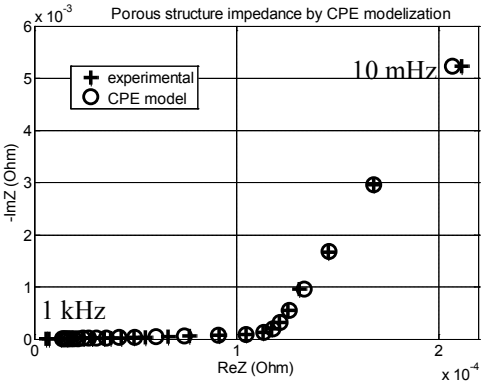

Figure 6 Porous structure impedance CPE model fitting

3) MP Model[5]

The MP model has been published in 2006. The idea of Hammar [5] was to group the n_i pores of the same individual impedance characteristics. The parameters Z_{pi}, R_{eli}, C_{dli} depend on the impedance of one pore and the number n_i of parallel pores in the group. Each group of pores can be modeled by a branch. The parallelization of each branch results in the impedance of the whole porous structure. The second interesting fact is that each pore of the branch owns the same (R_{eli}/n_i, $n_i C_{dli}$) characteristics. Then a single pore model with (R_{eli}, C_{dli}) parameters is sufficient for representing the behavior of each branch (Fig. 11). Thus impedance of porous structure can be expressed thanks to the parallelization of single pore impedance expression(2).

$$Z_{PorousStructure} = \sqrt{\frac{R_{el1}}{j\omega C_{dl1}}} \times \coth(\sqrt{j\omega C_{dl1} R_{el1}}) \,//\, ... \qquad (2)$$
$$... \,//\, \sqrt{\frac{R_{elk}}{j\omega C_{dlk}}} \times \coth(\sqrt{j\omega C_{dlk} R_{elk}})$$

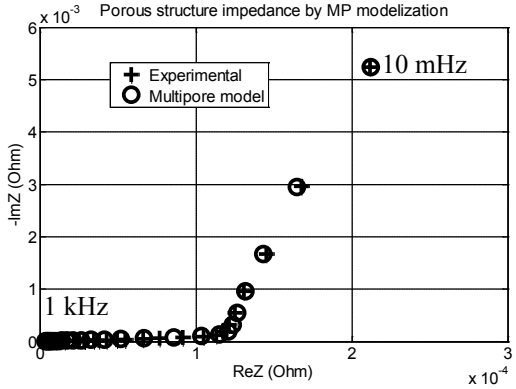

Figure 7 Porous structure impedance MP model fitting

The LF precision of MP model is much better than with single pore model (see Fig. 6) and equivalent at CPE

model (see Fig. 8). The issue of equivalent circuit on CPE model (see Fig. 7) has been settled as the impedance models just uses R and C components. The major appearing drawback is the mathematical difficulties to extract parameters. As a matter of fact the model equation is far much complicated than with CPE models because of the branches parallelization.

D. EDLC Ageing [2]

Fig.8 represents the influence of 2.8V 60°C ageing on the EDLC 10 mHz capacitance and the resistance R_0 (defined as the real part of EDLC impedance when the imaginary part of EDLC impedance is null). This study has been launched on 2 manufacturers since the 12 December and is still running. Capacitance is calculated at a frequency of 10 mHz (3).

$$C(\omega) = \frac{-1}{Im(Z_{EDLC}(\omega)) \times \omega} \quad (3)$$

Where ω is the pulsation and $Im(Z_{EDLC}(\omega))$ is the imaginary part of EDLC impedance. As presented in Fig. 1 porosity blocking is accompanied by capacitance loss. The increase of R_0 is characteristic of connections defects evolution and binding agent ageing. Other models can be applied to get more ageing parameters (single pore, CPE, MP). A paper studying ageing interpretation by MP model has been submitted to the IPEC conference in Vietnam [6]. The acceptation date is the 15 September.

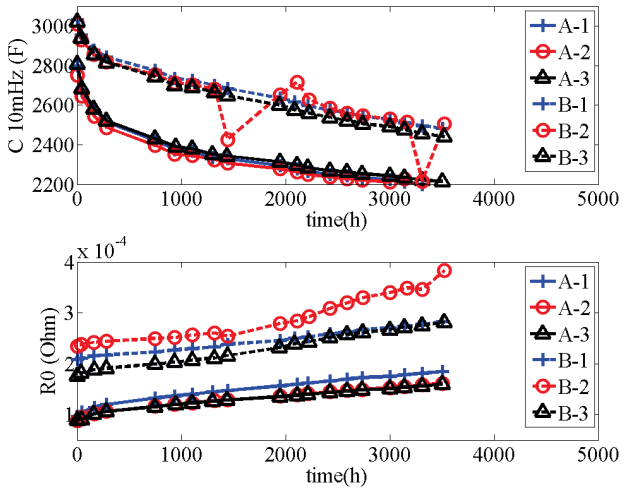

Figure 8 EDLC parameters evolution with ageing

III. Conclusions and Perspectives

The first year of PHD has been dedicated to the conception and building of experimental test benches. Important investments have been made (28 tracks programmable CC/ DC/ CP supply, high power cycling bench and thermal oven acquisitions). Then the second year has been dedicated to publications. An article has been presented in conference REVET (Renewable Energy and VEhicular Technologies) 2012. It won the best paper award. The aim of this article was to present and compare EDLC impedance models in term of low frequency fitting precision and ageing monitoring quality. The multipore (MP) model has shown a lot of qualities in both domains. Thus it will be used for ageing results and interpretations. A review with more precisions is about to be submitted to IEEE IES [7]. The first experimental results on EDLC floating ageing (constant temperature and EDLC voltage) have been collected and interpreted. An article has been written and submitted to a conference with the first ageing interpretations by MP model. The next step is to include the particular ageing constraints encountered in the personal ground transports environment. Interpretation of difference between simple floating ageing and ageing caused by ground transports constraints (temperature changes, DC-DC conversion effects) will be done and constitutes the major point of interest of PHD.

Publication Works

[1] R. German, P. Venet, A. Sari, O. Briat, and J. Vinassa, "Comparison of EDLC impedance models used for ageing monitoring," in *Renewable Energies and Vehicular Technology (REVET), 2012 First International Conference on*, march 2012, pp. 224 –229. **Published**

[6] R. German, P. Venet, A. Sari, O. Briat, and J. Vinassa, "Interpretation of electrochemical double layer capacitors (supercapacitors) floating ageing by multi-pore model," in *The 10th International Power and Energy Conference IPEC 2012*, 12 - 14 December 2012. **Submitted**

[7] R. German, P. Venet, A. Sari, O. Briat, and J. Vinassa, "Review on electrochemical double layer capacitors ageing impacts and comparison on ageing monitoring impedance models," *IES*, 2012. **Submission**

Other References

[2] R. D. Levie, "Electrochemical response of porous and rough electrodes, advances in electrochemistry and electrochemical engineering," *Wiley Interscience*, vol. 6, pp. 329–397, 1967.

[3] H.-K. Song, H.-Y. Hwang, K.-H. Lee, and L. H. Dao, "The effect of pore size distribution on the frequency dispersion of porous electrodes," *Electrochimica Acta*, vol. 45, no. 14, pp. 2241 – 2257, 2000.

[4] R. Kotz and M. Carlen, "Principles and applications of electrochemical capacitors," *Electrochimica Acta*, vol. 45, no. 1516, pp. 2483 – 2498, 2000.

[5] A. Hammar, P. Venet, R. Lallemand, G. Coquery, and G. Rojat, "Study of accelerated aging of supercapacitors for transport applications," *IEEE trans on Industrial Electronics*, vol. vol 57, p. pp.1473–1478, 2010.

Département "Méthodes pour l'Ingénierie des Systèmes", Ampère (UMR 5005)
Journée scientifique, St Bernard, 11 juillet 2012

Approximation, control and Application of Infinite Dimensional Systems

Hao LU
Michael Di Loreto, Laboratoire Ampère

Abstract–
In this work, we focus on the control and approximation of a class of infinite dimensional systems. More precisely, we address the approximation problem of distributed delays, and its application for the control of some infinite dimensional systems. Contributions of this work include effective methods for distributed delay approximation, its applications to systems inversion, and for pole placement of fractional systems.

Resumé–
Dans ce travail, nous nous intéressons au le contrôle et à l'approximation d'une classe de systèmes de dimension infinie. Plus précisément, nous abordons le problème de l'approximation de retards distribués, et son application pour le contrôle de certains systèmes de dimension infinie. Les contributions de ce travail incluent le développement de méthodes efficaces d'approximation de retards distribués, et leur application à l'inversion des systèmes, et au placement de pôles pour des systèmes fractionnaires.

1 INTRODUCTION

Infinite dimensional systems appear in industrial control and engineering applications, such as transmission line, teleoperated robot arm [5], heat conduction [28], flatness of heavy chain systems [21], flexible robot arm [9], flexible marine risers [8] etc. Generally speaking, infinite dimensional systems, such as time-delay systems or distributed parameter systems, can be represented by partial differential equations with some boundary conditions. Based on an input-output approach, we can associate with this partial differential equation a transfer function. Such a transfer function is, in general, a fraction of analytical functions, like $T(s) = \frac{\cosh\sqrt{2s}}{\sinh\sqrt{2s}}$. Thus they are difficult to be realized in state-space form, and their analysis (spectral properties, dynamics, controllability, etc.). From state-space domain is more complex than the finite dimension case. This complexity requires tools of approximation for simulation analysis and control of this class of dynamical systems.

A large field of works have been done to explore different approximation techniques for infinite dimensional systems. A general framework for lumped approximation was proposed by Vidyasagar and Anderson [26]. Fourier transform techniques have been investigated in [7], numerical discretization methods [23] , spectacle approximation [6]. In my thesis we will define the class of infinite dimensional systems, and we will develop tools control synthesis of such systems. The central element in what follows is an input-output convolution operator called distributed delay. distributed delay appear in Smith's predictor control [25], control of time-delay systems, some model of fluid systems, such as [24]. In this thesis, we address the approximation problem of distributed delays, and propose a general methodology to achieve such an approximation. We introduce a general framework for input-output approximation of distributed delay. The approximation realization was made on lumped systems and on a subclass of distributed delays. With previous objectives, we enclose the approximation problem into the Weiner algebra BIBO-stable systems, using the graph topology. This corresponds to the weakest topology for which feedback stabilization is a robust property. Moreover, we work on norm convergence over this algebra, which is a Banach algebra.

We also work on two applications where distributed delay plays a central role. The first one is the stable inversion problem. Stable inversion is commonly used in many control applications, such as trajectory planning, tracking, optimal control, or feed-forward control. In this thesis, we will introduce a generic stable inversion procedure for linear time invariant systems, using lumped and distributed delays. The solution is BIBO-stable and causal in the time domain. This solution is an approximated inverse of the plant: After a finite time, the error on exact inversion for this approximation will be identically zero. The second application is the finite spectrum assignment for infinite dimensional systems. This problem aims to find a static feedback control such that a finite number of eigenvalues of the closed-loop systems are arbitrarily located in the complex plane, while the others disappear.

2 CONTEXT OF THESIS

A *Approximation of distributed delay*

The first part of my Ph.D., I was concerned with approximation of distributed delay with the development of effective algorithms for the numerical computation of distributed delay.

Let us introduce it through an example. Consider the unstable plant $T(s) = \frac{\mathrm{e}^{-s}}{s-1}$. we take a controller $C = \frac{2\mathrm{e}}{1+2\frac{1-\mathrm{e}^{-(s-1)}}{s-1}}$, which admits the state space realization $u(t) = -2\int_0^1 \mathrm{e}^{\tau}u(t-\tau)\mathrm{d}\tau + 2\mathrm{e}y(t) + v(t)$, where $v(t)$ is the reference input (see Figure 1). The closed-loop system will be stable, with a closed-loop pole in $s = -1$. From a numerical point of view, can we realize the controller? In other words, how to implement $\int_0^1 \mathrm{e}^{\tau}u(t-\tau)\mathrm{d}\tau$?

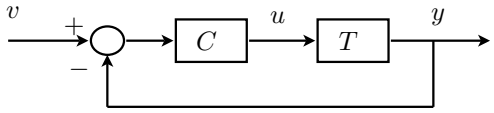

Figure 1: closed-loop feedback system

The interest for the use of distributed delays in the stabilization of time delay systems appears in the pioneering work of Olbrot [20]. With the generalize algebraic methods issued from linear systems in finite dimensional spaces to time-delay systems, Kamen et al. [10] first introduce a general mathematical setting for the control, and in particular for the stabilization, of time-delay systems. This mathematical framework was formalized in [3] by the introduction of the Bézout ring of pseudopolynomials. These works were mainly focused on stabilization. More generally, one can be interested in spectrum assignment by feedback. For linear time-delay systems, a necessary and sufficient condition to achieve spectrum assignment is the spectral controllability. In such a synthesis of feedback, distributed delays appear to play a central role in [18] and [27]. Finite spectrum assignment generalizes the principle of Smith's predictor for dead-time systems [25] to general systems with delays, which can be stable or unstable. Distributed delays appear also in the characterization of equivalence transformations [1]. Robustness issue and optimization [4], robustness for input-delay systems [19] or finite time control [11] are other topics where distributed delays play a central role.

A distributed delay is a linear input-output convolution operator of the form

$$y(t) = (f * u)(t) = \int_0^{\vartheta} f(\tau)u(t-\tau)\mathrm{d}\tau, \qquad (1)$$

where ϑ is a strictly positive and finite real number, while kernel $f(\cdot)$ is a continuous function with support in $[0, \vartheta]$. An input-output causal convolution system is a dynamical system described by an equation of the form (1) where $y(\cdot), u(\cdot)$ and $f(\cdot)$ are said to be the output, input and kernel of the map, respectively. For BIBO-stable systems, the kernel function f lies in the $\mathscr{A}$ [22]. Let $\mathbb{I}_{a,b}$ be a finite closed interval in $\mathbb{R}_+$, for some bounded reals a and b, $0 \leq a < b$. We define $\mathscr{K}(\mathbb{I}_{a,b})$ as the set of real valued functions $g(\cdot)$ of the form

$$f(t) = \begin{cases} f_{\mathbb{I}_{a,b}}(t) & t \in \mathbb{I}_{a,b} \\ 0 & \text{elsewhere} \end{cases}, \qquad (2)$$

where

$$f_{\mathbb{I}_{a,b}}(t) = \sum_{i\geq 0}\sum_{j\geq 0} c_{ij}t^j\mathrm{e}^{\lambda_i t}, \qquad (3)$$

for some c_{ij} and λ_i in $\mathbb{C}$, the sums being finite. In other words, $f_{\mathbb{I}_{a,b}}$ is a finite linear combination of exponential-polynomials type functions, and it is in particular a continuous function. In other words, a distributed delay is a causal convolution with a rational kernel having a finite support. Any distributed delay admits a Laplace transform denote by $\mathscr{G}$, corresponding to the finite Laplace transform of its kernel $f \in \mathscr{K}(\mathbb{I}_{\vartheta_1,\vartheta_2})$. Any distributed delay can be decomposed into a finite sum of distributed elements, called elementary distributed delays [17]. For this, we define the elementary distributed delay by the complex valued function $\theta_\lambda(\cdot) \in \mathscr{K}(\mathbb{I}_{0,\vartheta})$, for some $\lambda \in \mathbb{C}$ and $\vartheta > 0$, by

$$\theta_\lambda(t) = \begin{cases} \mathrm{e}^{\lambda t} & t \in [0, \vartheta] \\ 0 & \text{elsewhere} \end{cases}. \qquad (4)$$

Its Laplace transform is

$$\hat{\theta}_\lambda(s) = \frac{1-\mathrm{e}^{-(s-\lambda)\vartheta}}{s-\lambda}, \qquad (5)$$

which is an entire function even in $s = \lambda$ where $\hat{\theta}_\lambda(\lambda) = \vartheta$. The distribute delay is useful in the control of infinite dimensional systems. But when λ is positive or zero in (5) , there will be a numerical stability problem. See Figure 2 the simulation block in Matlab. In [17] we give the solution

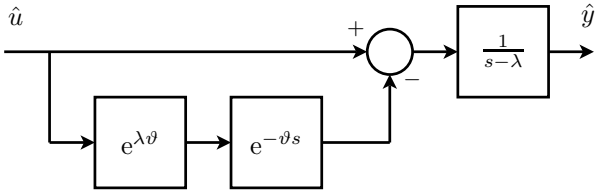

Figure 2: Realization of an element distribute delay.

of this problem. The idea is using the sum of the elementary distributed delay with $\lambda < 0$ approximate the elementary distributed delay with $\lambda \geq 0$. That is to say we can approximate an increasing exponential function by sum of decreasing exponential function. The approximation to the kernel of elementary distributed delay is $\mathrm{e}^{\lambda t} \approx \sum_{i=1}^{n} \mathrm{e}^{-i\alpha t}$, $\alpha > 0$. And this approximation has a convergence property in $\mathscr{L}_1$-norm. For example, in the Laplace transform

of the distribute delay $\frac{1-e^{-(s-1)}}{s-1}$ can be approximated by $\sum_{i=1}^{n} \frac{1-e^{-(s-\lambda_i)}}{s-\lambda_i}$ where $\lambda_i < 0$. The simulation result of Gain bode diagram can be seen in Figure 3

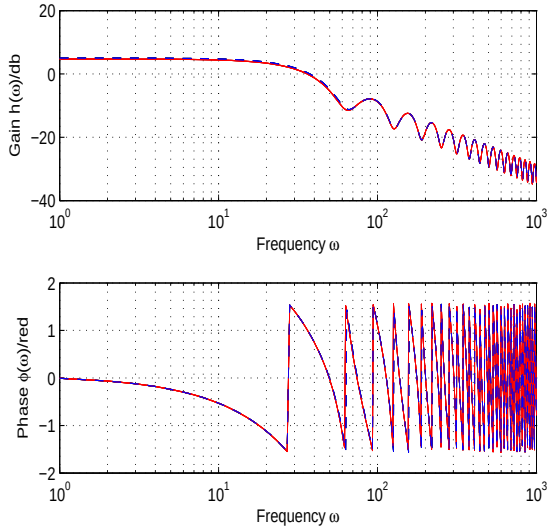

Figure 3: Bode diagram of $\hat{\theta}_1(j\omega)$ and its kernel approximation $\hat{\theta}_{1,\mathrm{app}}(j\omega)$, with order $n = 5$.

B Applications of distributed delay

In this part, I will introduce two applications of distributed delay. One is system inversion (or stable inversion), and the other is finite spectrum assignment.

B.1 Stable inversion

Stable inversion is introduced in this section, which is the first application of the distributed delay. Stable inversion and model matching are commonly used in many control applications, such as trajectory planning, tracking, optimal control, and feedforward control. We will introduce a generic model matching and stable inversion procedure for linear time invariant systems, using lumped and distributed delays. The solution is BIBO-stable and causal in the time domain. This solution is an approximated solution: After a finite time, the error on this approximation will be identically zero. Constructive algebraic procedures and simulation results are carried out for SISO systems [15], and for MIMO systems systems[16].

The problem of exact model matching can be stated as below: Given a plant $T(s)$ and the matching model $T_m(s)$, we want to find a precompensator $C(s)$, so that the transfer function of the resulting system $G(s) = C(s)T(s)$ has a prespecified model $T_m(s)$. In other words, we want to find a precompensator $C(s)$, for which the error of the system e should be zero, as shown in Figure.4.

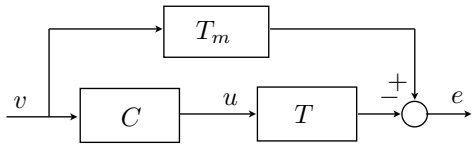

Figure 4: Model matching problem

A novel finite time model matching has been proposed in this thesis. The precompensator $C(s)$ satisfies the identity

$$E(s) = T_m(s) - T(s)C(s), \tag{6}$$

where the model matching error $e(t)$ has a finite time support. The impulse response of the model matching error is expected to vanish in finite time. It should be noticed that the precompensator $C(s)$ is BIBO-stable, and is causal. It admits also a state-space representation.

In the stable inversion problem, the specified model is $T_m = I$. In this problem, the error with respect to the exact inversion vanishes in a finite time. Both stable inverse and precompensator are BIBO-stable and causal. Constructive algebraic procedures were proposed in [15] for SISO systems, and in [16] for MIMO systems.

B.2 Finite Spectrum Assignment

Another application of distributed delay is related to the Finite Spectrum Assignment (FSA). FSA is a static feedback control, such that n eigenvalues of the corresponding closed-loop system are located at an arbitrarily preassigned set of points in the complex plane, while the others are automatically cancelled. In general, infinite dimensional systems have an infinite number of eigenvalues. FSA is one of the control methods for infinite dimensional systems, which give a complete procedure and which has the scope to do a link between control synthesis of finite dimensional systems and those of infinite dimension. For many different control problems of the infinite dimensional systems, such as optimal control and trajectory planning, the basic assumption is stabilization, and FSA is a very effective method. This method was first developed by Manitius and Olbrot [18]. And there are lots of literatures that show the solution to the FSA of infinite dimensional systems (or time-delay systems), such as in [27] [20] [2]. In this thesis, I will introduce a state feedback control for the FSA.

We consider the following system

$$\begin{cases} \dot{x}(t) = \sum_{i=1}^{k} E_i \dot{x}(t - i\vartheta) + \sum_{i=0}^{k} A_i x(t - i\vartheta) \\ \qquad\qquad + \sum_{i=0}^{k} B_i u(t - i\vartheta) \\ y(t) = \sum_{i=0}^{k} C_i x(t - i\vartheta) + \sum_{i=0}^{k} D_i u(t - i\vartheta) \end{cases} \tag{7}$$

where $x(t) \in \mathbb{R}^n$ is the instantaneous state, $u(t) \in \mathbb{R}^m$ is the control input, $y(t) \in \mathbb{R}^p$ is the output. The matrices A_i, B_i, C_i, D_i, E_i are real with adequate dimensions. All delays are commensurable to $\vartheta > 0$. The systems arise in the boundary control of certain hyperbolic partial differential equations. We are interested in the static feedback control.

$$\begin{aligned} u(t) &= \int_0^{\vartheta_1} f_1(\tau)u(t-\tau)\mathrm{d}\tau + \int_0^{\vartheta_2} f_2(\tau)x(t-\tau)\mathrm{d}\tau \\ &+ \int_0^{\vartheta_3} f_3(\tau)\dot{x}(t-\tau)\mathrm{d}\tau + ... \\ &+ \sum_{i=0}^{k} g_{1_i}x(t-i\vartheta) + \sum_{i=0}^{k} g_{2_i}\dot{x}(t-i\vartheta) + ... \end{aligned} \quad (8)$$

The Laplace transform of the control (8) is

$$\hat{u}(s) = \hat{F}_1(s)\hat{u}(s) + \hat{F}_2(s)\hat{x}(s) \quad (9)$$

where $\hat{F}_1 \in \hat{\mathscr{G}}$, $\hat{F}_2 \in \hat{\mathscr{G}} + \mathbb{R}[s, \mathrm{e}^{-\vartheta s}]$. The characteristic polynomial of the system (8) with the control (9) can be given as following:

$$\Psi_{bf}(s) = \det \begin{bmatrix} s(I_n - \hat{E}) - \hat{A} & -\hat{B} \\ -\hat{F}_2 & I_m - \hat{F}_1 \end{bmatrix}. \quad (10)$$

where $\hat{A}(\mathrm{e}^{-\vartheta s}) = \sum_{i=0}^{r} A_i \mathrm{e}^{-i\vartheta s}$, $\hat{B}(\mathrm{e}^{-\vartheta s}) = \sum_{i=0}^{r} B_i \mathrm{e}^{-i\vartheta s}$,$\hat{F}_1 \in \hat{\mathscr{G}}, \hat{F}_2 \in \hat{\mathscr{G}} + \mathbb{R}[s, \mathrm{e}^{-\vartheta s}]$. So the finite spectrum assignment problem is equivalent to determine $F_1 \in \hat{\mathscr{G}}$, $F_2 \in \hat{\mathscr{G}} + \mathbb{R}[s, \mathrm{e}^{-\vartheta s}]$ such that

$$\Psi_{bf}(s) = \prod_{i=1}^{n}(s - \alpha_i), \quad \alpha \in \mathbb{C}.$$

For this problem we find the solution and have approach to obtain the control $u(t)$. We have discovered the solution and have found the approach to obtain the control $u(t)$ to this problem. Please refer to [14][13] for the detailed algorithm of FSA. We will just give an example in here.

Take the plant

$$\begin{cases} \dot{x}(t) = \dot{x}(t-1) + u(t) \\ y(t) = x(t) \end{cases} \quad (11)$$

and the control of the system is

$$\begin{aligned} u(t) &= -u(t-1) + u(t-2) - \int_0^1 u(t-\tau)\mathrm{d}\tau \\ &- 2x(t-1) + x(t-2) - 2\dot{x}(t-2) \\ &+ \dot{x}(t-3) + v(t). \end{aligned}$$

where $v(t)$ is the reference input and the simulation result can be saw in figure 5

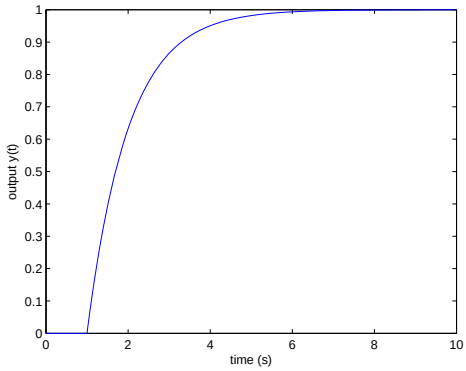

Figure 5: the step response in time $1s$

3 CONCLUSION AND PERSPECTIVES

We have presented here the results (so far) reached in this thesis. We find the approach to implement the distributed delay, and solve the problem of stable inversion, model matching and finite spectrum assignment of infinite dimensional systems where distributed delay play a central role.

For the future work we will continue the work in stable inversion by using stable feedback control in state space representation, and research how to implement the control in the finite spectrum assignment since the control of FSA always complex and not easy to realize.

The work carried so far has led to several publication [15] [12], in preparation publication [17] [16][14][13].

References

[1] Z. Artstein. Linear systems with delayed control: a reduction. *IEEE Trans. on Autom. Contr*, 27:869–879, 1982.

[2] D. Brethé and J. J. Loiseau. An effective algorithm for finite spectrum assignment of single-input systems with delays. *Mathematics and Computers in Simulation*, pages 339–348, 1989.

[3] D. Brethé and J. J. Loiseau. A result that could bear fruit for the control of delay-differential systems. *in 4th IEEE MSCA, Maleme, Greece*, 1996.

[4] H. Dym, T. T. Georgiou, and M. C. Smith. Explicit formulas for optimally robust controllers for delay systems. *IEEE Trans. on Autom. Contr*, 44:656–669, 1995.

[5] M. Fliess and H. Mounier. On a class of linear delay systems often arising in practice. *Kybernetika*, 37:295–308, 2001.

[6] L. Greengard and P. Lin. Spectral approximation of the free-space heat kernel. *Applied and computational harmonic analysis*, 9:83–97, 2000.

[7] G. X. Gu, P. P. Khargonekar, and E. Bruce lee. Approximation of infinite-dimensional systems. *IEEE Trans on Autom contr*, 34:610–618, 1989.

[8] B. V. E. How, S. S. Ge, and Y. S. Choo. Active control of flexible marine risers. Journal of sound and vibration. *Naval Underwater Systems Center*, 320:776–785, 2009.

[9] C. W. Jen, D. A. Johnson, and R. Gorez. A reduced-order dynamic model for end-effector position control of a flexible robot arm. *Mathematics and computers in Simulation*, 41:539–558, 1996.

[10] E. W. Kamen, P. P. Khargonekar, and A. Tannenbaum. Proper stable bezout factorizations and feedback control of linear time-delay systems. *Int. J. Contr.*, 43:837–857, 1986.

[11] M. Di Loreto. Finite time model matching for time-delay systems. *IFAC Workshop on Time-Delay Systems, Aquila, Italy*, 2006.

[12] M. Di Loreto, J-F. Lafay, J. J. Loiseau, and H. LU. On the structure at infinity for linear time-delay systems. *9th IFAC Workshop on Time Delay Systems*, 2010.

[13] H. Lu and M. Di Loreto. Feedback control for the finite spectrum assignment. *parper for submit in 2013*.

[14] H. Lu and M. Di Loreto. finite spectrum assignment for infinite dimensional systems. *parper for submit in 2013*.

[15] H. Lu and M. Di Loreto. On Stable Inversion for Linear Systems. *18th IFAC World Congress Milano (Italy)*, pages 6651–5565, 2011.

[16] H. Lu and M. Di Loreto. Finite Time Model Matching for Multivariable Linear System. *submit to IFAC workshops 2013, Grenoble, France*, 2013.

[17] H. Lu, M. Di Loreto, D. Eberard, and J. P. Simon. Approximation of distributed delay. *submit to journal Systems & Control Letters*, 2012.

[18] A. Z. Manitius and A. W. Olbrot. Finite spectrum assignment problem for systems with Delays. *IEEE Trans. on Autom. Contr.*, 24:541–553, 1979.

[19] S. Mondié, S. Niculescu, and J. J. Loiseau. Delay robustness of closed loop finite assignment for input delay systems. *IFAC Workshop on Time-Delay Systems*.

[20] A. W. Olbrot. Stabilizability, detectability and spectrum assignment for linear autonomous systems with general time delay. *IEEE Trans. On Autom. Contr*, 23:887–890, 1978.

[21] N. Petit and P. Rouchon. Flatness of heavy chain systems. *Proceedings of the 41st IEEE, USA*, pages 362–367, 2002.

[22] R. F. Curtain qnd H. J. Zwart. An introduction to infinite dimensional linear systems theory. *Springer-Verlag, New York*, 1995.

[23] A. Quateroni and A. Valli. Numerical approximation of partial differential equations. *Automatika*, 42:177–188, 2008.

[24] L. Sinègre, N. Petit, and P. Ménégatti. Distributed delay model for density wave dynamics in gas lifted wells. *Proceedings of the 44th IEEE conference on dicision and control, and the european control conference, Seville, Spain*, pages 7390–7397, 2005.

[25] O. J. M. Smith. A controller to overcome dead time. *Inst. Soc. Amer. J*, 6:28–33, 1986.

[26] M. Vidyasagar and B. D. O. Anderson. Approximation and stabilization of distributed system by lumped systems. *Systems & Control Letters*, 12(95–101), 1989.

[27] K. Watanabe. Finite spectrum assignment and observer for multivariable systems with commensurate delays. *IEEE Trans. on Autom. Contr*, 31:542–550, 1986.

[28] M. Necati Ozisik. *Heat conduction*. A wiley-interscience publication, New York, 1980.

Modeling, Ageing and Health Monitoring of Metallized Films Capacitors used in Power Electronics Applications

Maawad MAKDESSI
Pascal VENET, Ali SARI (Ampère, UMR 5005, Université de Lyon)
Marcello ITURRIZ (Airbus)
Gregor MASSIOT (EADS)

***Abstract*— Capacitors are one of the most widely used forms of electronic components. A careful choice of a capacitor for a particular application and an adequate installation in the circuit will assure a good life service. Since half of the electric equipement failures are caused by capacitors degradation, interest for capacitor "Health monitoring" function reveales to be very strong. Eventhough metallized polymer films capacitors proved to be more reliable components than cheap electrolytic capacitors in aerospace applicatitions, given the risk of infalamation in the case of a default, improving the dependability of these components and monitoring their health conditions are fundamental to the availability of systems in which they are employed. Two approaches should be considered: reliability and diagnostic. The major concern in the 'reliability' process is to monitor and analyze the degradation modes which requires knowledge of in-service use and life cycle environmental and opperational conditions. Diagnostic, through adequate measurements must ensure analysis of the component aging, an essential step to predict tolerances and capacitor performance and its remaing lifetime. The final interest has been growing in monitoring the ongoing health of the system in order to predict failures and provide warnings in advance of catastophic failure. Thus, the goal of these studies is to provide a basic understanding of the degradations modes of metallized films capacitors and to develop new techniques of health monitoring to enable pronostics for power electronics systems.**

***Résumé*— Compte tenu de leur capacité à stocker de l'énergie électrique sous forme de charges électrostatiques, les condensateurs sont utilisés dans de nombreuses applications de l'électronique de puissance. Le choix d'un condensateur bien adapté au système peut s'avérer primordial car il est responsable, dans certaines applications, de la majorité des défaillances et donc d'arrêts intempestifs de systèmes très critiques. Malgré que les condensateurs à films métallisés s'avèrent des composants plus fiable que les condensateurs electrolytique dans les applications aeronautiques, mais compte tenu du risque d'inflammation en cas de défaut, l'amélioration de la sureté de fonctionnement de ces composants et la surveillance de leurs états de santé sont donc fondamentales pour la disponibilité des systèmes dans lesquels ils sont employés. Deux approches en interaction forte afin de concourir à l'objectif d'amélioration de la sûreté de fonctionnement de ces composants, sont considérées : la fiabilité et le diagnostic. La préoccupation majeure dans la démarche 'fiabilité' est de suivre et d'analyser les défauts et le vieillissement des composants. Le diagnostic par l'intermédiaire de mesures et de méthodes adéquates doit assurer la détection des pannes ou du vieillissement des composants ; la finalité recherchée étant de prévoir les défaillances grâce à l'application d'une maintenance prédictive. Par ailleurs, l'analyse du vieillissement des composants est primordiale pour prévoir les tolérances et les performances du condensateur ainsi que sa durée de vie. Les axes majeurs de cette thèse s'avèrent être l'identification des mécanismes et modes de défaillances des condensateurs films métallisés d'une part et la surveillance de leur état de santé d'autre part.**

I. INTRODUCTION

A. *Project background*

Aerospace industry is slowly moving towards a more electric airplane, where electrical systems are gradually replacing hydraulic technologies. Electrical technology offers some strong advantages such as cost, efficiency, power on demand as well as relative

ease of maintenance. The inverter constituting the subject of our study (cf. Fig. 1), is not dedicated to a particular application. It can be placed into the airplane cabin subjected to well known environmental conditions (electrical, thermal), as well as outside the plane (wing for example) which imposes more stringent conditions of use (humidity, electromagnetic interferences …) not known accurately. Our inverter is supplied with an HVDC network +/- 270 V, which requires an AC power generation, rectification and filtering blocs.

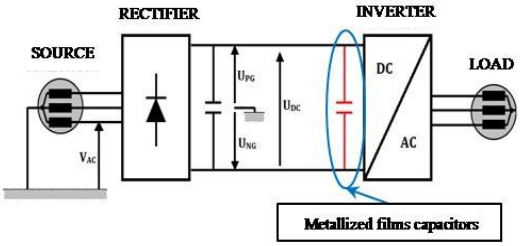

Fig. 1. Scheme of the inverter under test

Our work focuses on the metallized films capacitors used as DC-link capacitors.

B. *Why the choice of metallized films capacitors?*

Capacitors are widely used in power electronic applications and the need nowadays is increasingly growing to have more robust devices, compact and able to withstand more stringent conditions of use. Although each type of capacitor has its own limitations, advantages and disadvantages, the films capacitor has the blend of proprieties that make it well suited for these applications. Unlike electrolytic capacitors, plastic films capacitors do not require a given polarization and behave well under high current and voltage conditions. Metallized films capacitors are a very interesting alternative to electrolytic capacitors and present higher reliability, higher RMS currents and small capacitance change regardless of applied voltage. Metallized films capacitors have been used since the 1950's and were coveted for their abilities of self-healing; defects such as pinholes, embedded foreign particles or even micro flaws in the dielectric material can lead to a localized breakdown of the film. Such a breakdown event results in the discharge of a portion of the stored charge with the development of a sudden localized temperature and pressure build-up. During this intense discharge, a puncture is developed in the dielectric material and the thin metallization layer near the defected site is rapidly vaporized and blown away and the site becomes electrically isolated. Thus, metallized film capacitors can undergo a large number of breakdowns with as only visible impact a slight drift of its electrical parameters. Polymer films are the preferred materials of choice for capacitive energy-storage applications thanks to their high dielectric breakdown strengths, low dissipation factors and good stability over a wide range of frequencies and temperatures. The most common plastic used as dielectric are respectively the polypropylene (*PP*) and the polyethylene Tereftalate also known as polyester (*PET*). Capacitors using these two different materials as dielectric should be tested in order to determine the most reliable type for our application.

II. Characterizations and Ageing Protocols

A. *Temperature dependence*

Metallized films capacitors are components whose characteristics vary with temperature and have a measurable influence on the entire circuit behavior. The ambient temperature considered for avionic applications extends over a range of -40°C to 70°C (up to 85°C in the component). This temperature sweep should be taken into account within the limits of possible for the metallized films capacitors studies.

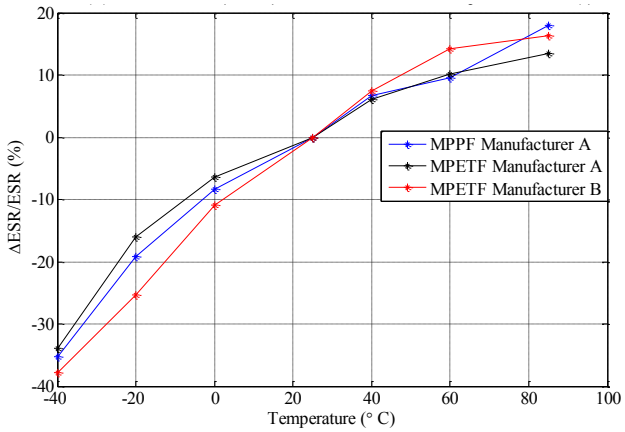

Fig. 2. Evolution of the equivalent serial resistor with the ambient temperature

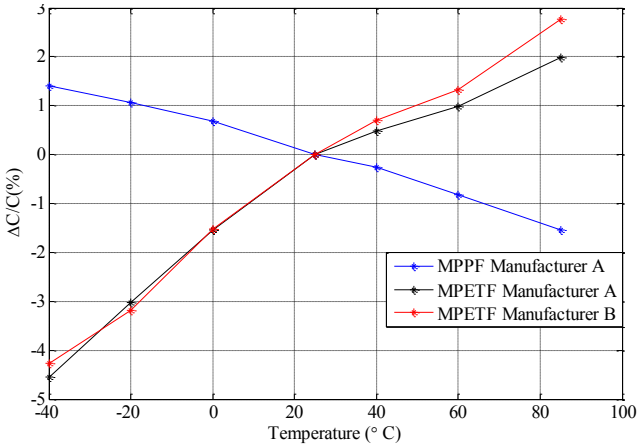

Fig. 3. Evolution of the capacitor capacitance with the ambient temperature

Fig. 2 and Fig. 3 show the evolution of the capacitor parameters with respect of the ambient temperature. It is of interest to note that as seen in Fig. 3, the capacitance do not behave the same according to the dielectric material that have been used. This difference is the mainly due to chemical composition of the

material itself. Polymers are separated into two main categories, polar and apolar dielectric; *PP* belongs to the apolar type, while the *PET* belongs to the polar group.

B. *Ageing protocols*

Ageing protocols have been defined, and are listed as follow:

- 'Floating ageing', at fixed temperatures and voltages. This kind of tests will allow us to deduce the accelerating ageing factors in function of the ambient temperature and the applied voltage.
- 'Ageing through cycling tests' – High current. This test constrains mainly the connection 'electrode-schoopage' of the capacitor.
- 'Ageing by superposing a ripple current with a DC voltage'. This test aims to characterize the individual impact of the amplitude and the frequency of the ripple current on the capacitor lifetime. It also subject the component to similar constraints encountered during a normal operation.

C. *First Ageing Results*

The first ageing test (1,1.U_N-85ºC) was launched for both types of metallized films capacitors (*PP* and *PET*). The components of test were selected to have the same ratings (0.68 µF-630V, 1µF-630 and 15µF-400V) but whose type (PP, PET) and/or manufacturer are different.

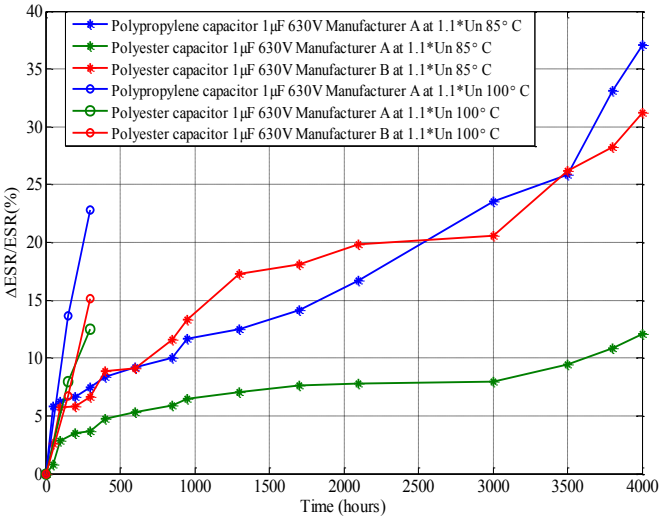

Fig. 4. Evolution of the ESR with ageing time

To study the influence of temperature and voltage on the lifetime of the capacitors, a second aging test was lunched (1,1.U_N-100ºC) for the types of cited previously. Fig. 4 and Fig. 5 show the evolution of the capacitor parameters in function of the ageing time. In fact, a capacitor is considered as inoperative when its equivalent serial resistance (*ESR*) reaches the double of its initial value and/or when its capacitance decreases of 20% from its original value. At this point, as seen in the Fig. 4 and Fig. 5, the ageing tests affect mainly the capacitor equivalent resistor; its capacitance remains almost constant. These evolutions are mainly due to the self healing properties of the metallized films capacitors as described in the previous section.

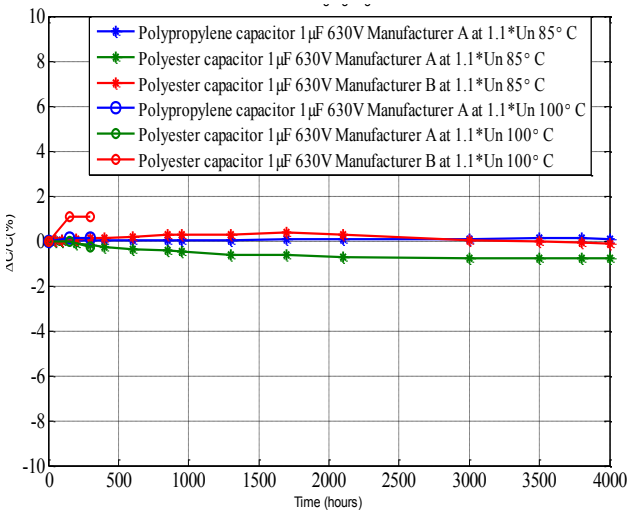

Fig. 5. Evolution of the capacitance with ageing time

'Ageing through cycling tests' and 'ageing by superposing a ripple current with a DC voltage' requires the use of a specific test bench and is described in the Fig. 6.

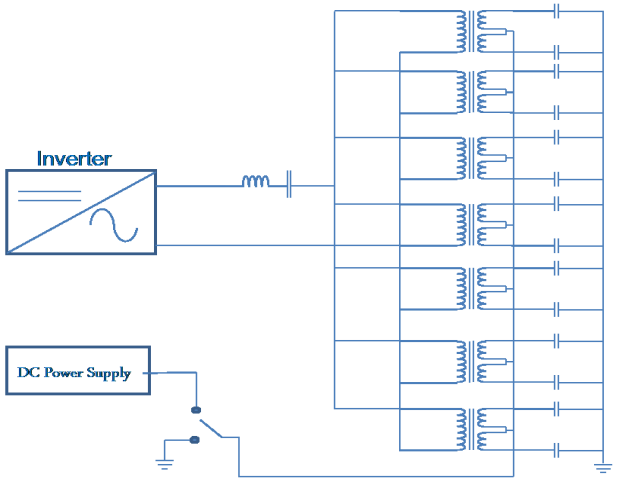

Fig. 6. Accelerated ageing test bench

This test bench is in the realization phase, and it should be operative at the end of July 2012.

III. METALLIZED FILMS CAPACITOR MODEL

Proper deign of metallized films capacitors requires an understanding of all parasitic parameters sources and their impact on circuit operation. Parasitic parameters could occur at low frequencies as well as at high frequencies and disturb substantially the behavior of the component. Many models have been developed in literature within frequency variation; Nyquist plot showed an imprecision in the parameters identification. Since the capacitor impedance is constituted of a real and an imaginary part, our proposed approach consists on applying the fitting algorithm on the complex expression of Z; Nyquist

diagram reflects well this approach.

Two different models have been developed depending on the dielectric material that has been used. Fig. 7 and Fig. 8 present the models thus developed respectively for metallized polypropylene and polyester films capacitors.

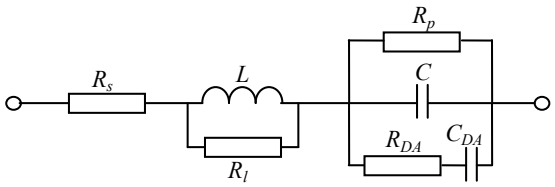

Fig. 7. Metallized polypropylene films capacitor model

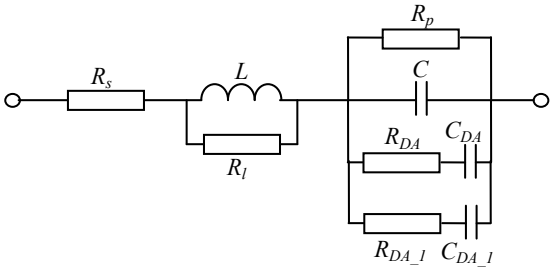

Fig. 8. Metallized polyester films capacitor model

Where R_s represents the contact and electrodes resistance; R_p is the parallel resistance taking into accounts the dielectric losses and leakage between the electrodes. C represents the nominal capacitance of the capacitor, while the inductance L in parallel with R_l represents the contribution due the skin and proximity effect. R_{DA}-C_{DA} refers to the dielectric absorption (DA) in the capacitor. DA is also called 'Capacitor Soakage, dielectric relaxation, or even residual charges, and is related to the remnant polarization trapped on dielectric interfaces, and is highly dependent on the dielectric material itself. In addition, some polarization of the dielectric may be due to physical charges accumulating on grain boundaries of polycrystalline materials, charges tunneling to the surface states at the plate interface, or the formation of electric domains. From an electrical circuit point of view, the extra polarization behaves like a set of additional series RCs time constants connected in parallel with the main capacitance. If a capacitor is charged for a long time and then briefly shorted, a residual voltage slowly builds up across its terminals and reaches a fixed percentage of its original value. This percentage referring to the DA of the capacitor can range from 0.02% for polypropylene up to 0.5% for polyester dielectrics. This phenomenon can affect in some cases the operation of some particular electronic devices and should be taken into account. Fig. 9 and Fig. 10 represent respectively the Nyquist diagrams of a metallized polypropylene (MPPF) capacitor 1µF-630V and a metallized polyester films (MPETF) capacitor 1µF-630V. The continuous line represent the experimental measurements, while the dots are the theoretical points calculated with respect to Fig. 7 and Fig. 8. The agreement between experimental points and theoretical plots is quite good which proves the accuracy of the model.

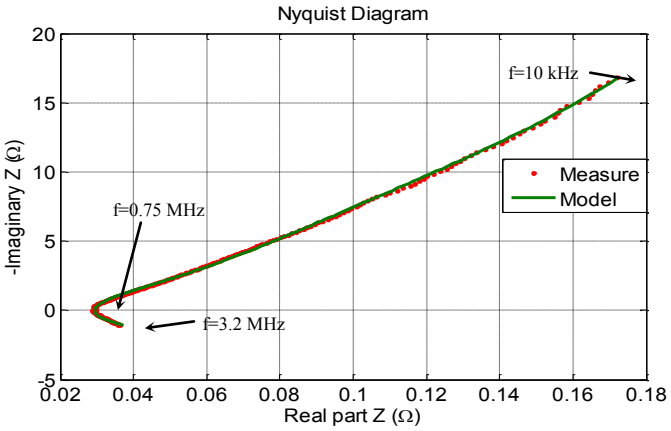

Fig. 9. Nyquist plot of MPETF capacitor 1µF-630V

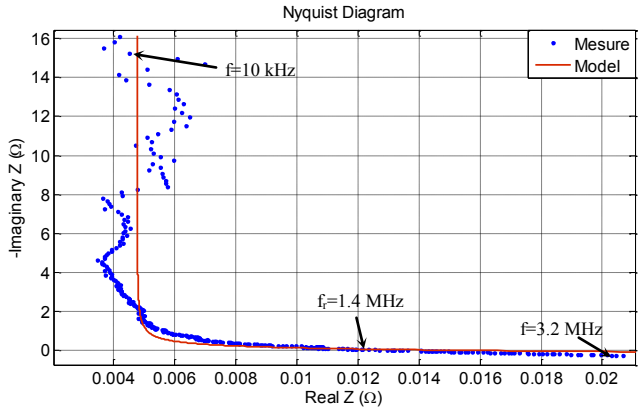

Fig. 10. Nyquist plot of MPPF capacitor 1µF-630V

IV. Conclusion and Perspectives

Identification results obtained with the proposed approach induces an accurate and simple technique for determining the capacitor parameters for a wide range of frequency and temperature. The results obtained are quite satisfactory and give a good idea about the DA in capacitors. Different phenomena, not taken into account in the described model, could occur at high frequencies and disturb substantially the capacitor behavior. Modeling at high frequencies should be the next step to do in our future work. Furthermore, as the ageing tests progress, the capacitor parameters will degrade, and thus we would be able to analyze and determine the failure modes taking place into the component. Once the capacitors reach their end of life, we can determine the ageing lows of the metallized films capacitor, and integrate them into the health monitoring phase.

References

[1] M. MAKDESSI, A. SARI and P. VENET, *'Modeling of Metallized Films Capacitor Impedance', IEEE – IECON 2012*

Hybrid Observer and Predictive Control Of DC-DC Power Converters

Ahmed-Rédha MEGHNOUS
Supervisors: Xuefang Lin-Shi and Minh-Tu Pham

***Abstract*—In this report, we are interested in the design of a hybrid observer for DC-DC power converter using port-hamiltonian modeling. Some theoretical results and an experimental implementation on a SEPIC converter are given. Our motivation to study such a converter is mainly due to its particular topology that includes observable and unobservable subsystems. Another aspect of or work focuses on the synthesis of a predictive hybrid control of the output voltage. Unlike other techniques, we show that stability in closed loop can be obtained with our approach.**

***Résumé*— Nous nous intéressons dans ce rapport au développement d'un observateur hybride pour les convertisseurs de puissance DC-DC en s'appuyant sur la modélisation hamiltonienne. Quelques résultats théoriques et une mise en œuvre expérimentale sur un convertisseur SEPIC sont donnés. L'étude d'un tel circuit est motivée par sa topologie particulière qui contient à la fois un mode de fonctionnement observable et une mode de fonctionnement inobservable. Un autre aspect de notre travail concerne la synthèse d'une commande prédictive hybride pour le control de la tension de sortie. Contrairement à d'autres techniques, nous montrons que la stabilité du système en boucle fermée peut être obtenu avec notre approche.**

I. INTRODUCTION

DC-DC converters are frequently encountered in lots of contexts. Power converters usually exhibit switching between several subsystems. Switched systems have been attracted considerable attention in control community recently and most of the efforts have been focused on stability, stabilization, controllability, and observability so far [3]. Switched systems may be viewed as higher-level abstractions of hybrid systems, obtained by neglecting the details of the discrete behavior. Informally, a switched system is composed of a family of dynamic subsystems (linear or nonlinear), and a rule, called switching law, that orchestrates the switching between them [7].

Among the theoretical properties of switched systems, observability is still subject of intense researches. This notion has different definitions in literature [7], and it depends on the knowledge of the switching control law. Observability of a switched system can be verified even if one or several of its sub-systems are not observable [3]. Moreover, the design of an observer of switched systems is well known to be a difficult problem. Unfortunately, despite of all the existing works, there is still none unified approach that tackles properly this field of research [2][6]. To overcome these concerns, many authors suggest to approximate the real system based on an averaged model [4]. The concept is to use a model constructed from the averaging of the different subsystems representing the process. Usually, this approximation leads to a bilinear model that makes observability easier to analyze. Unfortunately the proposed techniques can be only applied within a specified frequency range.

Generally, while hybrid observers are proposed, subsystems are supposed to be fully observable and switching is treated as a disturbance. While some modes are not observable, only a few solutions exist in the literature and allow the estimation of the entire state.

One of the challenges of our work is the design a hybrid observer for DC-DC power converters including unobservable subsystems. At the end of the first year, we have proposed a sliding mode observer based on an averaged model and proved its stability with port-Hamiltonian formalism. This observer was

validated in practice on a SEPIC converter (Single Ended Primary Inductor Circuit). Then, this observer was extended to estimate the load resistor. To our best knowledge, only one hybrid observer proposed by [2] in 2011 deals with modes fully unobservable. Having said that its implementation on real power converters seems quite difficult especially in closed loop. One of our contribution was to modify this work in order to propose a two mode switched observer that estimates the states even both subsystems are unobservable in classical sense of Kalman. We shown that the observer stability is guaranteed thanks to a Lyapunov function found by port-Hamiltonian formalism.

The second point of our research work concern the design of predictive control methodologies based on averaged and hybrid approaches dedicated to DC-DC converters [5]. A predictive deadbeat control has been developed in our lab and successfully implemented on a SEPIC converter [1]. This kind of control is intuitive and easy to put into practice but the stability in closed loop is not guaranteed. Therefore, we have developed a new Lyapunov based control of the output voltage where the stability of the closed loop is ensured. This control was successfully validated on in practice.

II. DC-DC POWER CONVERTER MODELING

The network modeling of DC-DC converters leads to manipulate a class of systems, called port-Hamiltonian systems. This modeling provides a unified framework for the physical description of different types of converters [8]. Let us consider the class of switched port-Hamiltonian system with dissipation that is given by

$$\begin{cases} \dot{x} &= P[J(q)-R]x + PB_q u \\ y_p &= PB(q)^T x \\ y &= Cx \end{cases} \quad (1)$$

where $x \in \Re^n$ is the state, $u \in \Re$ is the control vector, $y_p \in \Re$ and $y \in \Re^p$ are the port and the measurable outputs, C is the output matrix, B_q is the input matrix, P is an invertible symmetric matrix, R is a positive semi-definite diagonal matrix called dissipation matrix and supposed independent of q and J is a skew-symmetric matrix called structure matrix. $q = q_1, \cdots, q_k, k \in \boldsymbol{N}$ is the switching input and $N = 2^k$ is the number of the possible configurations.

The Hamiltonian is given by

$$H(x) = \frac{1}{2} x^T P^{-1} x \quad (2)$$

It represents the stored energy in the system. It will be used as a candidate Lyapunov function for the following.

The approximation (1) with an averaged model gives a bilinear model as

$$\begin{cases} \dot{x}_a = -PRx_a + P\sum_{i=1}^{N}[J_i(q_i)d_i]x_a + P\sum_{i=1}^{N} B_i(q_i)d_i u \\ y = Cx_a \end{cases} \quad (3)$$

x_a is the averaged state vector and d_i is the cycle duty.

III. OBSERVABILITY AND OBSERVER DESIGN

In this part, we present two observers. The first is a sliding mode observer based on averaged modeling and the second is a switched observer taking into account unobservable subsystems. Observability criteria are given in both cases.

Observability of the averaged bilinear system (3) can be investigated using the following definition.

Definition 1: The bilinear system (3) is said to be generically observable if

$$rank(O) = n \quad (4)$$

with $O = [O_1; O_2; \cdots; O_n]^T$ *where* $O_1 = C$ *and* $O_i = [O_{i-1}R; O_{i-1}J_1; \cdots; O_{i-1}J_N]^T$, *i=2,…,n.*

The following sliding mode observer is proposed in this report to estimate the unmeasured states in the power converter model.

$$\dot{\hat{x}}_a = -PR\hat{x}_a + P\sum_{i=1}^{N}[J_i(q_i)d_i]\hat{x}_a + P\sum_{i=1}^{N} B_{q_i} d_i u + PK\, sign(y - C\hat{x}_a) \quad (5)$$

$\hat{x}_a$ is the estimated of the averaged state vector x_a and *K* is the observer gain vector.

If $K = GC(x_a - \hat{x}_a)$, where $G \in \Re^{n\times 1}$ a gain vector such as GC and R-GC are semi-definite positive matrices, then the observer (5) is stable.

One can use the Lyapunov function:

$$V = \frac{1}{2} e_x{}^T P^{-1} e_x$$

to prove the last statement. Moreover, an extended observer is proposed to estimate the load resistor. Observer error in both observers is independent of the cycle duty, which means independent of the control input.

Our hybrid observer approach relies on the work of [2]. The main idea is to collect information from observable states of each mode and restitute all the states after the occurrence of a number of switching considered enough to obtain an observable system in hybrid sense. Different definitions exist for hybrid observability. It depends on knowledge of the discrete state, class of the system and hybrid time trajectory.

For switched linear systems, one can note that the definition introduced by [2] appears to be the most interesting and useful. Observability is considered over an interval independently of switching times. Moreover, observability of subsystems or modes is not required.

For the proposed hybrid observer, we considered a switching output as $y = C_q x$ and subsystems are not necessary observable in a classical sense. Each subsystem can have its own output. For DC-DC power converter consider the following switched observer:

$$\dot{\hat{x}}(t) = P[J(q) - R]\hat{x}(t) + B_q u + PW_q F_w^q C_{q-1}\xi(t) + PZ_q F_z^q C_q e(t) \quad (6)$$

where $e(t) = x(t) - \hat{x}(t)$ and $\xi(t) = e^{(P[J(q)-R]-F_q)(t-t_q)} Z_{q-1} Z_{q-1}^T e(t_q^-)$ with $F_q = P(W_q F_w^q C_{q-1} + Z_q F_z^q C_q)$. Z_q and W_q are matrices with suitable dimensions designed such that to isolate observable and unobservable states. t_q is the switching time. t_q^- is the time instant just right before switching. Recalling the common Lyapunov function $V = \frac{1}{2} e^T P^{-1} e$ and Lasalle invariance principle, asymptotic stability of this observer is guaranteed if $Z_q F_z^q C_q$ is chosen to be positive semi-definite and $\left\| W_q F_w^q C_{q-1} \right\| < \frac{1}{\delta}$ where δ is a lower bound of $(t - t_q)$.

IV. CONVERTER CONTROL

For this part, we consider the following class of averaged model:

$$\dot{x} = P[J_1 + dJ_2 - R]x + PBu \quad (7)$$

Where J_1 and J_2 are skew symmetric matrices. d is the cycle duty and takes the values between 0 and 1.

The reference trajectory is given by

$$\dot{x}_{ref} = P[J_1 + dJ_2 - R]x_{ref} + PBu \quad (8)$$

Consider the Lyapunov function:

$$V = \frac{1}{2}(x - x_{ref})^T Q P^{-1}(x - x_{ref}) + \frac{1}{2} S d^2 \quad (9)$$

With Q a weighting matrix and S a positive scalar.

To have $\dot{V} \le 0$, the dynamic of the control input must satisfy

$$\dot{d} = -\frac{1}{S}(x - x_{ref})^T Q(J_2 + \frac{1}{d} J_1)(x - x_{ref}) \quad (10)$$

Unlike the deadbeat control where there is not any proof of stability, this control law ensures the stability of the system in closed loop.

Two hybrid control approaches are proposed in our work. One is based on the oversampling of the switched model and the minimization a cost function to determine the adequate switching time over the real sampling time. The second technique is based on Lyapunov theory and can be assimilated to an optimal control.

V. APPLICATION TO SEPIC

DC-DC power converter can have an output voltage greater than, less than or equal to the input voltage Fig.1. Unlike the buck-boost converter, the SEPIC can maintain the same polarity and the same ground reference for the input and output [6]. It has a true shutdown mode: when the switch is turned off, its output drops to 0 V. Some typical applications of such a converter include digital cameras, cellular phones, CD/DVD players, PDAs and GPS systems. SEPIC model is a fourth order with four storage elements (two capacitors and two inductors) and one switching element. The switching element represents the control input and gives a switching behavior to the converter. Four sensors are needed to control the SEPIC. To reduce the volume and the cost of the converter manufacturing, it is important to use observers in order to reduce the sensor number. In this work, a SEPIC converter is considered with only the output voltage sensor. In experimentation on the real SEPIC circuit, the developed algorithms for observation and control are implemented on a dSpace dS1104 controller board. Data recording is performed within the Control Desk environment.

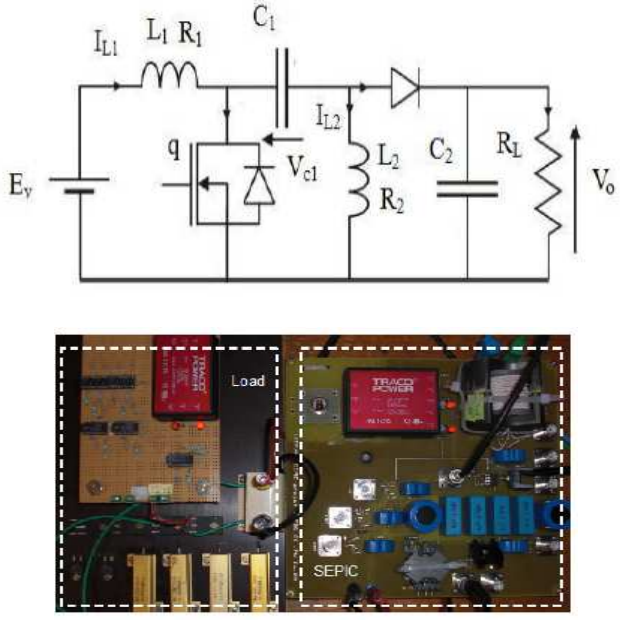

Fig.1. SEPIC Converter

Fig.2 and Fig.3 show the observation of the current I_{L1} with the averaged model extended sliding mode observer in simulation and experimentation with a

load resistor variation. Fig.4 shows the observation of the same current with the hybrid observer in simulation. Fig.5 and Fig.7 illustrate the output voltage controlled by a Lyapunov based control of the averaged model when the reference varies from 15v to 20v in simulation and practice respectively. Fig.6 and Fig.8 show the same controlled output when the load resistor varies from $44\,\Omega$ to $22\,\Omega$ in simulation and practice respectively. Fig.9 and Fig.10 represent the voltage output controlled in simulation by the two proposed hybrid controls: predictive control with oversampling and Lyapunov based hybrid control. For these two last controls, load resistor is changed at t=0.15s and the reference at t=0.4s.

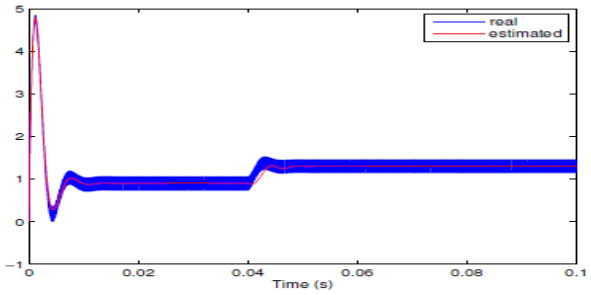

Fig.2. Observation of the current I_{L1} with the ESM observer in simulation

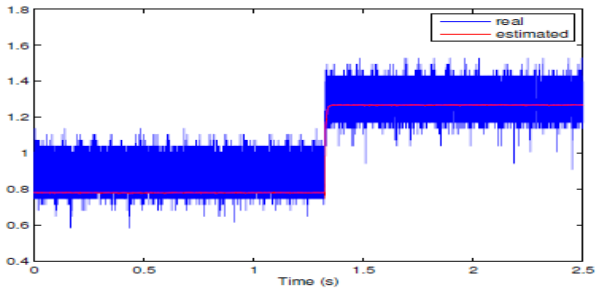

Fig.3. Observation of the current I_{L1} with the ESM observer in experimentation

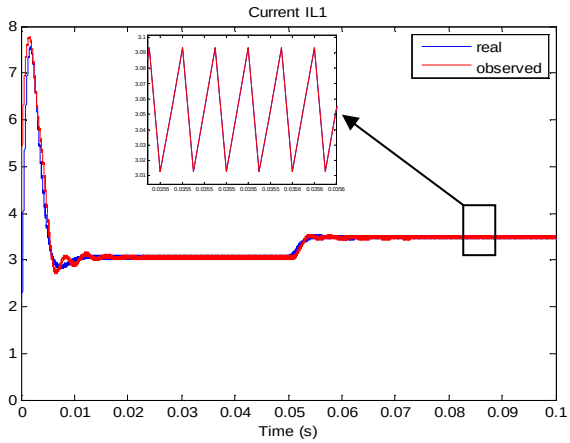

Fig.4. Observation of the current I_{L1} with the hybrid observer

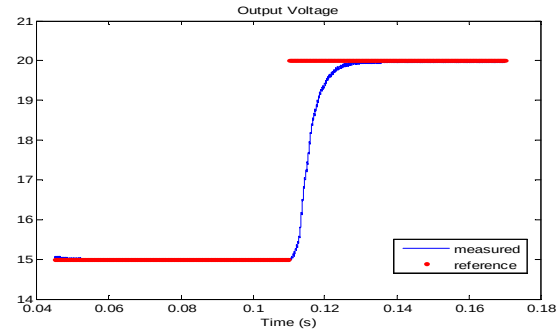

Fig.5. Voltage output (Simulation 1)

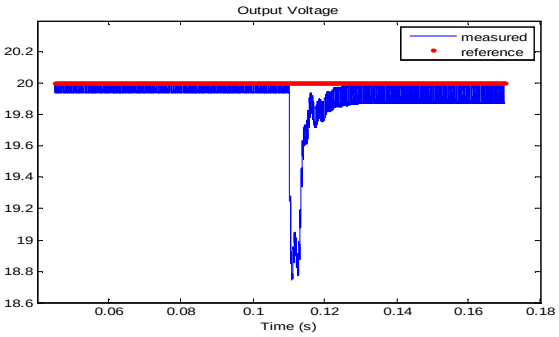

Fig.6. Voltage output (Simulation 2)

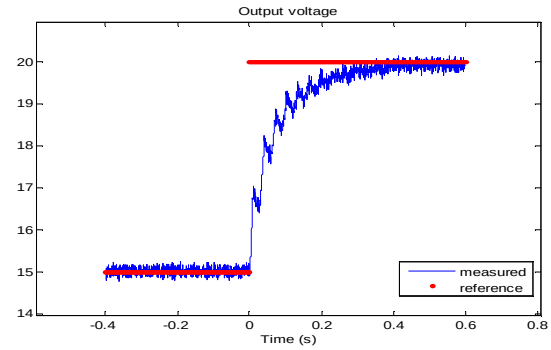

Fig.7. Voltage output (Experimentation 1)

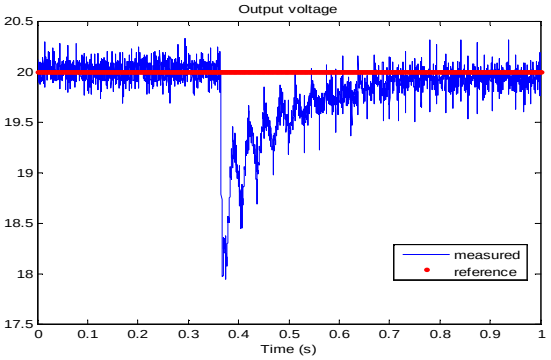

Fig.8. Voltage output (Experimentation 2)

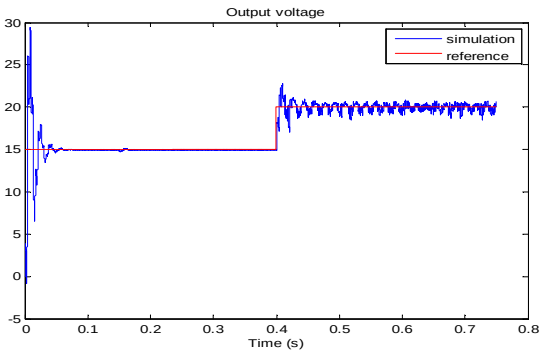

Fig.9. Predictive control with oversampling

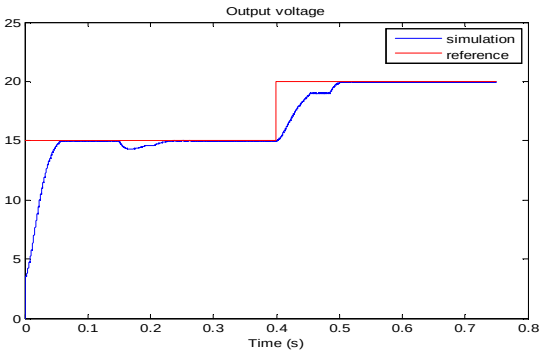

Fig.10. Lyapunov based hybrid control

VI. CONCLUSION AND PERSPECTIVES

During these two years of the thesis, we have proposed two observers for switched system: an averaged model sliding mode observer with an extension to estimate the load resistor and an original hybrid observer for DC-DC power converters. Both observers were validated in simulation but only the first one was validated in practice.

Recently, we have started a study about control design of power converter. Until now, a Lyapunov based control using averaged model has been developed and validated in simulation and practice. For this control law, a proof of stability in closed loop has been found. Two hybrid control methods are still under development: One is a predictive control based on the oversampling of the hybrid model and the second is an optimal control based on Lyapunov theory.

Future work consists in validating the switched observer in practice in open and closed loops. Since electrical systems have fast dynamics, the advantage to use a hybrid approach over an averaged approach is still limited. For the reason, we will consider to a class of switched systems with slow dynamics such as pneumatic systems. Perspective works for the control design consists in proposing a control technique based on sliding mode theory. Also, we will work up on the development of predictive control laws for hybrid models.

REFERENCES

[1] L. Nan, Digital Control Strategies for DC/DC SEPIC Converters towards Integration, Ph.D thesis, INSA de Lyon, 2012.

[2] A. tanwani, H. shim and D.Liberzon, Observability for Switched Linear Systems: Characterization and Observer Design, Automatica, 2011.

[3] S. Zhao and J. Sun, Controllability and observability for time-varying and non linear control, vol 20, 2010, pp 1313-1325.

[4] A. Jaafar, P. Lefranc, E. Godoy, X. Lin-Shi, A. Fayaz and N. Li, Experimental validation with a control point of view analysis of the sepic converter, IEEE Industrial Electronics Society Conference, Porto, Portugal, 2009.

[5] M. Baja, D. Patino, H. Cormerais, P. Riedinger and J. Buisson, Hybrid control methods for a Single Ended Primary Inductor Converter (SEPIC), European Control Conference , Budapest, Hungary, 2009.

[6] J.P. Barbot, M. Djemai and N. Manamanni, State Observer and Observability Conditions for a Class of Hybrid Continuous-Discrete Dynamic System, 46th IEEE Conference on Decision and Control, New Orleans, LA, 2007, pp 708-713.

[7] M. Babaali and M. Egerstedt, Observability of switched linear systems, HSCC 2004:Hybrid system: computation and control, Philadelphia, PA, vol 2993, 2005.

[8] A.J. Van Der Schaft and B.M. Maschke, Port-Hamiltonian systems: network modeling and control of nonlinear physical systems, Dynamics and Control, 2004, pp 1-38.

Energetic Optimization of Conventional, Electric and Hybrid Vehicles and its Application on Eco-Driving

Felicitas Mensing
Eric Bideaux, AMPERE-INSA Lyon, Rochdi Trigui, IFSTTAR

***Abstract*—In the transportation sectors a lot of research is devoted to reduce fuel consumption and emissions. Eco-Driving is an immediately applicable way to improve system efficiency in vehicles and refers to the behavior of the driver to optimize his fuel consumption. With the work of this thesis the optimal operation of conventional, electric and hybrid vehicles will be discussed. Using numerical optimization algorithms the maximum potential of eco-driving for passenger vehicles will be analyzed. The results will be used to contribute to the development of effective driver assistant systems for eco-driving.**

***Résumé*—Dans le secteur des transports les ingénieurs cherchent des nouvelles méthodes qui réduisent la consommation d'essence et la production d'émission. L'éco-conduite est une méthode utilisée par les conducteurs à fin d'augmenter l'efficacité du véhicule. Dans cette thèse le fonctionnement optimal des véhicules conventionnels, électriques et hybrides est étudié. En utilisant des méthodes numériques, nous déterminons l'économie d'énergie pouvant être réalisée grâce à l'éco-conduite. Les résultats sont ensuite utilisés pour le développement d'un système d'assistance à l'éco-conduite.**

I. INTRODUCTION

The transportation sector is a major producer of greenhouse gas emissions. Fuel prices are constantly growing while non-renewable fossil fuels are becoming scarce. To solve these problems researchers are looking for ways to reduce fuel consumption and emissions in the transportation sector. On one hand, new, more fuel efficient, drive train technologies are developed. On the other side, research on optimal vehicle use, such as vehicle operation and communication, is showing potentials to reduce fuel consumption.

In passenger vehicles energy is often wasted. An immediately applicable way to reduce fuel consumption and emissions for passenger vehicles is to adapt the use of the vehicle to the system functionality. Vehicle efficiency is not constant over its operating range but depends on the vehicle chassis and the losses in each component in the drive train. It is therefore strongly dependent on vehicle velocity and acceleration. The behavior of a driver that minimizes fuel consumption is often referred to as eco-driving.

Most countries offer eco-driving courses. But Beusen [1] has shown that fuel consumption is only reduces for a short time period after taking the course. In literature we can find many works on driver assistance systems with the goal to reduce fuel consumption. Most of these consist of a display that gives advice on more efficient vehicle operation to the driver ([2]). Haptic devices, like the active accelerator pedal ([3]), where the resistance of the accelerator pedal increases with acceleration, have also been developed. Other systems designed for eco-driving store information while driving and present a report with tips for improvement to the driver after the trip ([4], [5]).

After an exhaustive literature search we did not find references of a driver assist system for eco-driving purposes that uses numerical optimization, taking into account the drive train components, to identify optimal vehicle operation. For the existing devices the recommended optimal vehicle operation is determined using rule based algorithms. With this approach the advice given to the driver is suboptimal and a maximum gain in fuel consumption cannot be achieved.

In this thesis work numerical optimization methods are developed to identify optimal operation for each specific vehicle configuration. This way the maximum potential gains of eco-driving can be determined. The algorithms can either be used in connection with a GPS to give a report and advice on the optimal driving

and possible fuel savings to the driver. On the other hand the identified optimal operations could also be used to develop vehicle specific eco-driving rules.

II. Approach

To identify the optimal operation the approach taken here was to develop vehicle models of each different drive train. Then an appropriate optimization method applicable to the different cost functions is chosen and applied to the problem. For real time implementation the computation time of the algorithm has to be considered in the choice.

The developed algorithm is used to identify the optimal velocity trajectory for given missions for the conventional, electric and hybrid vehicle. With this the drive-train dependency of optimal operation and most important eco-driving factors will be identified.

The results will be verified in experimental settings on an engine test bench and a chassis dynamometer. This will identify discrepancies between the backward vehicle simulation and real vehicle operation. With this the maximum potential of eco-driving is discussed. Finally the results will be used in the development of a driver assistance system to reduce fuel/energy consumption.

III. Work Progress

A. Modeling

For optimization purposes an 'inverse' vehicle model was developed. In a vehicle drive train the power usually flows from the internal combustion engine (or other power source in the case of the electric or hybrid vehicle) to the wheels, where it propels the vehicle. In an 'inverse' approach the operation of the energy source is computed given the vehicle operation.

Three different drive trains were modeled: the conventional, the electric and the hybrid vehicle.

1) The Conventional Vehicle

The chassis was modeled using the resistance forces which are a sum of the aerodynamic drag, the rolling resistance and the grade resistance forces. The force at the wheel can then be calculated by

$$F_{wheel} = F_{roll} + F_{aero} + F_{grade} + F_a \quad (1)$$

where F_a=ma represents the acceleration force. Given the vehicle speed and acceleration the wheel torque and speed can be calculated by

$$T_{wheel} = F_{wheel} * R_{tire} \quad (2)$$

$$\omega_{wheel} = v / R_{tire} \quad (3)$$

with the tire radius R_{tire} and the vehicle speed v.

Modeling the final drive, the gear box, the clutch and auxiliaries the engine operation can be identified with

$$T_{eng} = T_{wheel} \frac{\eta_{FD}^{\alpha} \eta_G^{\alpha}}{R_{FD} R_G} + P_{aux} / \omega_{eng} \quad (4)$$

$$\omega_{eng} = \max(\omega_{idle}, \omega_{wheel} k_G k_{FD}) \quad (5)$$

where α=sign(T_{wheel}), ω_{idle} represents the engine idle speed, R_{FD} is the final drive ratio with an efficiency of η_{FD} and R_G is the gear ratio with an efficiency of η_G. In the calculation of the optimal operation the gear is always chosen to be optimal. Using an engine efficiency map the fuel consumption is computed as a function of vehicle speed and acceleration.

2) The Electric Vehicle

Usually, an electric vehicle drive train does not contain a gear box. The electric motor operation can therefore be calculated given the vehicle operation and the final drive ratio. Experimentally identified loss maps are used to model the electric machine. With this the power required by the electric battery is given as a sum of the electric motor output power, the losses of the electric motor and the auxiliary power:

$$P_{batt} = P_{EM} + P_{EMloss} + P_{aux} \quad (6)$$

The battery is modeled as a simple circuit with one resistance which changes its value dependent on the direction of current flow and battery state-of-charge (SOC). With this the electric energy consumption can be identified as a function of vehicle speed, acceleration and battery SOC.

However, since the changes in resistance in the battery were negligible with respect to the rest of the system losses for a wide range of battery SOC, the battery SOC was assumed to stay constant for a trip.

3) The hybrid vehicle

A hybrid vehicle is a vehicle that contains two or more power sources. Most hybrid vehicles on the road today combine an internal combustion engine with an electric motor/generator and a battery. These hybrid vehicles are called hybrid electric vehicles (HEV). Hybrid drive trains known today combine two different power sources in three different configurations: the parallel, the series and the power-split configuration.

In a first approach we started with the simulation of a series hybrid vehicle for simplicity. In further work the most common hybrid vehicle on the road today was modeled: the Toyota Prius. This is a power-split hybrid vehicle.

In modeling the operation of a hybrid vehicle it is not only important to simulate each component of the vehicle but to identify and model the control strategy.

For the series hybrid vehicle a simple on/off rule based energy management strategy was simulated. Using [6]

the energy management of the Toyota Prius vehicle was identified and included in the power-split vehicle model. With this, two different hybrid vehicle drive trains were modeled and their fuel consumption and battery state can be identified as a function of vehicle speed, acceleration and battery SOC.

B. Optimization

The system under consideration can be described with two states: the vehicle speed v and the distance x driven by the vehicle. For optimization purposes the dynamics of the system can be described by a set of discrete equations:

$$x_{i+1} = x_i + v_i \Delta t + a_i \Delta t^2 \quad (7)$$

$$v_{i+1} = v_i + a_i \Delta t \quad (8)$$

The cost of a mission is defined by the energy consumed for a given trip. In the case of a conventional vehicle this is the fuel, for the electric vehicle the electric energy used. The cost function to be minimized is specified by:

$$J = \sum_{t=0}^{t=t_f} J_i(t) \quad (9)$$

To identify the gain of eco-driving and compare optimal operation to general driving, normal driving has to be defined at first.

1) Constraint Specification

In this work standard drive cycles and real-life cycles were used to define normal driving. In order to achieve a fair comparison a vehicle mission has to be defined and constraints on the optimization have to be fixed. Here, trip constraints, road constraints and traffic constraints were defined.

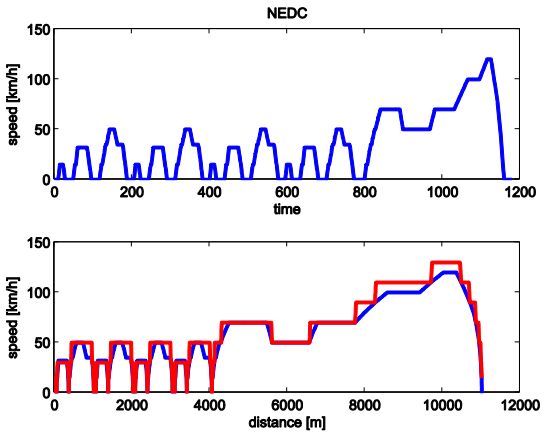

Fig.1. NEDC drive cycle

In Fig. 1 the New European Drive Cycle (NEDC) can be seen. In the first plot the vehicle speed is shown as a function of time, in the second plot the vehicle speed as a function of distance (in blue).

Given the cycle data in vehicle speed as function of time the trip constraints are defined in distance, velocity and time:

$$x(0) = x_0; x(t_f) = x_f; v(0) = v_0; v(t_f) = v_f; t_f = T \quad (10)$$

As road constraints maximum speed limits were assigned as a function of distance. Knowing the route these could be identified using road data. Here the original vehicle speed was used to identify a speed limit. The resulting maximum speed constraint can be seen in Fig. 1 and is defined by

$$v(x_k) \le v_{\max}(x_k) \quad (11)$$

In an urban setting it becomes difficult to perform eco-driving since our vehicle speed is bound to vehicle operation of the traffic. Due to the complexity of traffic constraints these are not considered in the following optimizations. However, a study on these was performed using experimental data, with vehicle following information of a radar equipped vehicle. In the study the effects of traffic and required safety distances are discussed. The study allowed us to submit a paper for review at Transportation Research Part D [7].

2) Optimization Methods

In literature trajectory optimization for road vehicles is a well-known problem. Several studies are found where the optimal velocity trajectory is identified considering energy used ([8–11]), fuel consumed ([12], [13], [14]), or trip time ([15]). Since the year 2000 the optimization problem has been applied to various applications. These include the development of adaptive cruise control ([16], [17]) where the average velocity is fixed, as well as the calculation of the optimal speed profile for city buses ([14]), where the trip is known. Some recent works have been using optimization techniques to compute the optimal velocity profile for electric fuel cell vehicles ([12]) and hybrid electric trucks ([13]).

Trajectory optimization problems can be solved using a variety of methods. Heuristic methods, like the genetic algorithm, can be used as well as direct methods like the Pontryagin's minimum principle ([9], [17]) and the dynamic programming method ([10], [18]) With heuristic methods it is often difficult to choose the appropriate initial parameters, and the evolutionary criterion. In addition the convergence might take a long time. Using calculus of variation with the Pontryagin's minimum principle is a very fast method. In this case an analytic formulation is necessary. Non-linearities and constraints are not simple to be implemented. Boundary value problems are often hard to be solved with this approach. With the dynamic programming (DP) method the computation time is exponentially growing with the

dimensions of the problem. It therefore takes more time to compute, particularly for high order problems. However the global optimum is identified and the method can be applied to any type of model type whether linear or non-linear.

Due to the complex constraints of the problem under consideration and the non-linear cost function, the dynamic programming method was chosen here. This method is based on the Principle of Optimality ([19]) stated by Bellman in the 1940s. Applying the principle the optimal solution is found by searching from the final state backward in time. In general the method brakes down a complex problem into smaller, simpler sub-problems which can be solved recursively. The method leads to a functional equation that can easily be solved with the digital computer.

Initially the problem was solved using a three dimensional dynamic programming approach [18] to satisfy all constraints (Eq. 10). The particular application of the method to this problem with the dependency of the three dimensions has allowed us to publish in the proceedings of the VPPC 2011 conference ([20]).

In order to reduce the computational time the method was reduced to a two dimensional DP by introducing a weighting factor in the cost function. This approach is similar to that of [10], while he never specifies how to evaluate the appropriate weighting factor to fix all constraints. In our work different ways to identify the weighting factor were studied and finally an iterative approach was used in combination with advanced root-finding methods. A paper describing the algorithm was submitted for review with Transportation Science [21]. With this method, given a vehicle mission with constraints, the optimal velocity trajectory for a given vehicle can be found.

Applying a multi-objective optimization method based on the dynamic programming method ([22]) allowed us to submit a paper, discussing the trade-off between fuel consumption and trip time for a conventional vehicle, for review with IEEE TVT Special Section [23].

The optimization for the particular case of the hybrid vehicle was treated. Since vehicle operation depends on vehicle velocity, acceleration and battery SOC this case is more complex. Due to the SOC dependency the optimization cannot be performed with the traditional DP method. To adapt to the system the method was used in a forward way, starting at t_0 and calculating all trajectories to t_f. Concerning this work an abstract was submitted to the VPPC 2012 paper call. Within the work on the hybrid drive train appropriate cost functions for optimization were studied including battery state of charge, fuel consumption, and altitude/ road grade.

C. *Verification/ Analysis*

To verify the algorithm and the gains of the resulting optimal trajectories the described original cycles with their optimal counterparts have to be tested in experimental settings.

For the conventional vehicle optimal velocity trajectories were computed for 4 different cycles for the example of the Peugeot 308 passenger vehicle. The results were tested in a hardware-in-the-loop setting on the engine test bench. The EP6 engine of the vehicle was operated in real time while simulating the rest of the vehicle. The resulting fuel consumption values show good results. A reduction in fuel consumption of 8% (for highway driving) up to 27% (for urban driving) was found.

For the case of the electric vehicle a test vehicle at IFSTTAR was used to test the resulting eco-driving profiles on a chassis dynamometer. In this case the real vehicle energy consumption is measured while a driver follows the defined speed profile. The vehicle is stationary while the resistance forces are simulated with the dynamometer on the wheels. The results of the test show a significant reduction of energy consumed between the eco-cycles and original profiles. The work on the electric vehicle has been proposed for presentation by an abstract sent to the EEVC 2012 conference.

To identify important eco-driving factors the optimal velocity trajectories were analyzed. It was found that fuel was reduced due to energy saved on aerodynamic drag, acceleration and braking. The optimal profile consists of three phases. It starts with a short, high acceleration phase, followed by a constant velocity section, where the speed is kept as low as possible, and a rather hard braking phase.

IV. Conclusion & Perspectives

With the current work it was found that eco-driving has a high potential to reduce fuel consumption. Important energy saving factors were identified.

In future work the optimal operation of the hybrid vehicle will be analyzed in depth. Tests on a chassis test bench of the Prius vehicle to verify the gains are scheduled in the near future. For the final thesis year we will put strong emphasis on the implementation of the developed algorithms. The development of an interface for a driver assistance system is envisioned.

References

[1] B. Beusen, S. Broek, T. Denys, et C. Beck, « Using on-board logging devices to study the longer-term imact of an eco- driving course », *Transportation Research Part D*, vol. 14, n°. 7, p. 514-520, 2009.

[2] M. van der Voort, « A prototype fuel-efficiency support tool », *Transportation Research Part C*, vol. 9, n°. 4, p. 279-296, 2001.

[3] A. Varhelyi, M. Hjaelmdahl, C. Hyden, et M. Draskoczy, « Effects of an active accelerator pedal on driver behaviour and traffic safety after long-term use in urban areas », *Accident Analysis and Prevention*, 2008.

[4] Fiat, « Fiat EcoDrive », *Fiat EcoDrive*, 16-avr-2012. [Online]. Available: http://www.fiat.co.uk/ecodrive/.

[5] J. N. Barkenbus, « Eco-driving: An overlooked climate change initiative », *Energy Policy 38*, p. 762-769, 2010.

[6] E. Vinot, J. Scordia, R. Trigui, B. Jeanneret, et F. Badin, « Model simulation, validation and case study of the 2004 THS of Toyota Prius », *International Journal of Vehicle Systems Modelling and Testing*, vol. 3, n°. 3, p. 139-167, janv. 2008.

[7] F. Mensing, E. Bideaux, R. Trigui, et H. Tattegrain, *Transportation Research Part D: Transport and Environment*, waiting for acceptance.

[8] A. B. Schwarzkopf et R. B. Leipnik, « Control of highway vehicles for minimum fuel consumption over varying terrain », *Transportation Research*, vol. 11, n°. 4, p. 279-286, 1977.

[9] Y. Saboohi et H. Farzaneh, « Model for developing an eco-driving strategy of a passenger vehicle based on the least fuel consumption », *Applied Energy*, vol. 86, n°. 10, p. 1925-1932, 2009.

[10] V. V. Monastyrsky et I. M. Golownykh, « Rapid computation of optimal control for vehicles », *Transportation Research Part B: Methodological*, vol. 27, n°. 3, p. 219-227, 1993.

[11] D. J. Chang et E. K. Morlok, « Vehicle Speed Profiles to Minimize Work and Fuel Consumption », *J. Transp. Engrg.*, vol. 131, n°. 3, p. 173-182, 2005.

[12] Guzzella, Lino et Sciarretta, Antonio, « Fuel optimal trajectories of fuel cell vehicles », presented at the International Mediterranean Modeling Multiconference, Bergeggi, Italy, 2004.

[13] T. van Keulen, B. Jager, D. Foster, et M. Steinbuch, « Velocity Trajectory Optimization in Hybrid Electric Trucks », presented at the American Control Conference, Baltimore, MD, USA, 2010.

[14] L. Nouveliere, M. Braci, et S. Mammar, « Fuel Consumption Optimization for a City Bus ». UKACC Control 2008, 2008.

[15] E. Velenis et P. Tsiotras, « Optimal velocity profile generation for given acceleration limits; the half-car model case », in *IEEE International Symposium on Industrial Electronics 2005, ISIE 2005, June 20, 2005 - June 23, 2005*, Dubrovnik, Croatia, 2005, vol. I, p. 361-366.

[16] E. Hellstroem, M. Ivarsson, J. Aslund, et L. Nielsen, « Look-ahead control for heavy trucks to minimize trip time and fuel consumption », *Control Engineering Practice*, vol. 17, n°. 2, p. 245-254, 2009.

[17] E. Hellstroem, J. Aslund, et L. Nielsen, « Design of an efficient algorithm for fuel-optimal look-ahead control », *Control Engineering Practice*, vol. 18, n°. 11, p. 1318-1327, nov. 2010.

[18] J. N. Hooker, « Optimal Driving for Single-Vehicle Fuel Economy », *Transportation Reserach-A*, p. 183-201, 1988.

[19] D. E. Kirk, *Optimal Control Theory: An Introduction*. Dover Publications, 2004.

[20] F. Mensing, R. Trigui, et E. Bideaux, « Vehicle trajectory optimization for application in ECO-driving », in *2011 IEEE Vehicle Power and Propulsion Conference (VPPC)*, 2011, p. 1-6.

[21] F. Mensing, E. Bideaux, R. Trigui, et B. Jeanneret, « Velocity Trajectory Optimization for Application in Eco-Driving - Reducing Computational Cost », *Transportation Science*, waiting for acceptance.

[22] A. Guigue, M. Ahmadi, R. Langlois, et M. J. Hayes, « Pareto Optimality and Multiobjective Trajectory Planning for a 7-DOF Redundant Manipulator », *Robotics, IEEE Transactions on*, vol. 26, n°. 6, p. 1094-1099, 2010.

[23] F. Mensing, E. Bideaux, et R. Trigui, « Velocity Trajectory Optimization for Application in Eco-Driving - Fuel Consumption versus Trip Time », *IEEE TVT Special Section*, waiting for acceptance.

Class D Amplifier Current Prediction for EMI Purpose

Roberto MRAD
Christian Vollaire, Professor of the Ecole Centrale de Lyon

***Abstract*— The impedance matrices are used to predict the EMI emissions of an integrated Class D audio amplifier. The method presented here, models the output passive parts of differential integrated switching amplifier with blocks represented by impedance matrices. The open circuit voltages of the integrated circuit are then used with the resulting impedance matrix for all the output passive parts, to predict the currents flowing in the system. For validation this method is applied on a Class D amplifier, EMI filter and speaker. The experimental results in blocks association and current prediction are validated up to 110 MHz.**

***Résumé*—La méthode de modélisation présentée dans cet article permet de prédire les spectres de courants d'un système électronique différentiel. Le système électronique considéré est décomposé en circuits élémentaires modélisés par des matrices d'impédances. L'association de ces blocs élémentaires permet de reconstruire le système. Ceci permet alors d'étudier l'impact fonctionnel de chacun des blocs et son influence CEM dans un système global. De plus l'assemblage des blocs permet l'obtention d'un modèle système compact pour des simulations CEM ultérieures.**

I. INTRODUCTION

Over the years, cell phones have become more and more complicated. Expert designers are introducing complex systems for more sophisticated functionalities. These are composed of calculation and power management circuits, fabricated in submicron technologies, calculating with extremely high speed (processors, controllers etc.), switching at high frequencies (DC-DC convertors) and mounted on a small area of a portable cell phone. This trend for size reduction also reduces also the supply voltage which leads to a better power efficiency. However, this smaller supply voltage reduces the noise margin which increases the system susceptibility to electromagnetic interference (EMI). As higher switching frequencies, lead to much conducted and radiated noise emissions, the ElectroMagnetic Compatibility (EMC) can no longer be neglected.

To study the EMIs, experts now study the already built systems and try to generate an equivalent EMI model. Indeed, a post-construction model can be useful, but it is not able to predict the frequency spectrum in order to solve the EMI problems before construction, which mean time to market and costs cannot be reduced. Designers therefore need an EMI predictive method to solve their problems at the early design stage, with good accuracy at high frequencies and with a short simulation time. In order to do that, the present method allows system integrators to use the already built parts of the system like integrated circuits (e.g. switching class D amplifiers), filters, speakers etc., and predict the behavior of their association. For example, if several filters and loads were modeled, the system integrator could determine which filter and load combination shows the best electromagnetic efficiency with a given power amplifier.

Here, the method used is applied on the passive output circuit of a differential class D audio amplifier (Fig.1). The different passive parts of the system are modeled with blocks, and each block is represented by an impedance matrix. The Blocs are then associated and one single impedance matrix is resulting for current prediction using the output voltages of the amplifier.

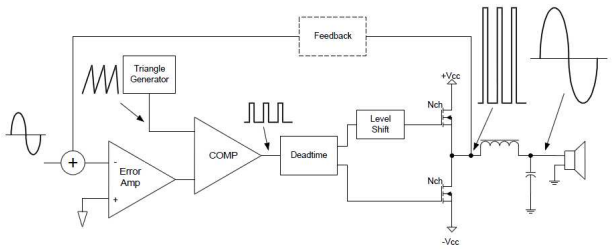

Fig.1. Class D amplifier architecture

II. METHOD PRINCIPALS

The present approach consists in decomposing a system with two active conductors and a ground plane in blocks (Fig.2). These blocks can then be associated in order to rebuild the behavior of the system as a single block. There are two types of block. The first represents the active blocks (Class-D amplifier and the DC-DC converter); the second, represents the passive blocks (filters, tracks, loads etc).

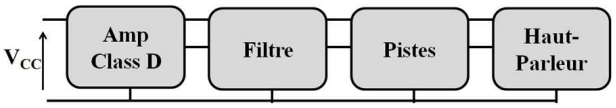

Fig.2. System decomposition into blocs

A. Modeling by impedance matrices

Since the class D amplifier has an H-bridge power stage and a differential output, each passive output block is considered as five ports box, because it has two voltages and two currents on the input as well as on the output, except the load (loudspeaker in this case). In fact, the load output cannot be electrically measured so the load is modeled as three ports bloc with only two voltages and two currents on its input. Then, each five ports block will be mathematically represented by a 4x4 impedance matrix, and the three port block (load) will be represented by a 2x2 impedance matrix (Fig.3).

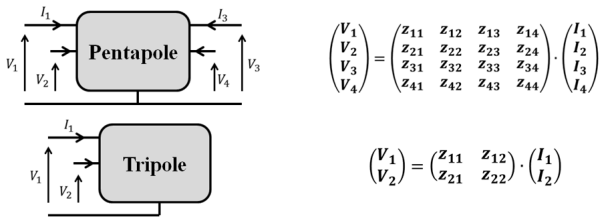

$$\begin{pmatrix} V_1 \\ V_2 \\ V_3 \\ V_4 \end{pmatrix} = \begin{pmatrix} z_{11} & z_{12} & z_{13} & z_{14} \\ z_{21} & z_{22} & z_{23} & z_{24} \\ z_{31} & z_{32} & z_{33} & z_{34} \\ z_{41} & z_{42} & z_{43} & z_{44} \end{pmatrix} \cdot \begin{pmatrix} I_1 \\ I_2 \\ I_3 \\ I_4 \end{pmatrix}$$

$$\begin{pmatrix} V_1 \\ V_2 \end{pmatrix} = \begin{pmatrix} z_{11} & z_{12} \\ z_{21} & z_{22} \end{pmatrix} \cdot \begin{pmatrix} I_1 \\ I_2 \end{pmatrix}$$

Fig.3. Blocks modeling by impedance matrices

Obtaining the impedance matrix consist in determining the diagonal and the cross elements in the following equation (1) when using a vector analyzer, or equation (1) for the diagonal elements and equation (2) for the cross elements when using an impedance analyzer. These impedances can be measured for post-construction modeling (impedance meter, vector analyzer etc.), or simulated for pre-construction modeling.

$$Z_{ij} = \frac{V_i}{I_j} \quad ; \quad (i = 1 \dots 4 \, ; j = 1 \dots 4) \tag{1}$$

$$Z_{ij} = \sqrt{Z_{jj}(Z_{ii} - Z_{ijsc})} \; ; \; (i = 1 \dots 4 \, ; j = 1 \dots 4 \, ; i \neq j) \tag{2}$$

Where Z_{ijsc} is the impedance seen at the *i* port when the *j* port is short-circuited.

B. Blocks association

Once the matrices of the different blocks in the considered sub-system are determined, they can be associated to rebuild the sub-system into a simple block modeled by a 2x2 impedance matrix. This resulting matrix contains the behavior of the whole sub-system including the defects of all the blocks. It also contains the impedances of the common and differential mode, as well as the mode conversion. The association techniques are presented in [1-3]. Two techniques can be distinguished; the first when associating two five ports blocks and the second is when associating a five ports block and a three ports block. Figure 4 shows the resulting system which contain the class D amplifier and the resulting passive block. This latter is modeled by a 2x2 impedance matrix.

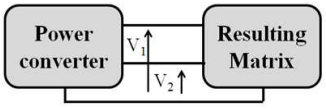

Fig.4. Resulting system after blocks association

C. Current prediction

Once the complete system is rebuilt as a simple matrix, this model is able to predict the current flowing in the system, using the input voltages (measured or simulated) and the resulting impedance matrix using equation (3).

$$\begin{pmatrix} I_1 \\ I_2 \end{pmatrix} = Z_R^{-1} \cdot \begin{pmatrix} V_1 \\ V_2 \end{pmatrix} \tag{3}$$

Note that, it is importance to measure the output voltages of the class D amplifier in the same time. This will allow a correct phase between the two voltages after doing the FFT (Fast Fourier Transform).

III. EXPERIMENTAL VALIDATION

This approach is applied on an EMI filter and a mobile phone speaker for validation. The amplifier is a test IC (Integrated Circuit) of class D audio amplifier mounted on a test board. The filter is recommended with the evaluation kit of an existing Class-D amplifier [4]. The load is a micro-speaker used in cell phones applications [5].

The impedance matrix of the Filter and the speaker are measured. Hereafter, the matrices are mathematically associated using the procedure presented in [1-3].

The output voltages of the class D amplifier are measured in the time domain, and not directly in the frequency domain, because the phase between the two voltages is needed for currents calculation. Hereafter, the FFT is applied to the measured voltages to obtain the frequency spectra. Finally, voltages spectra are multiplied with the inverted resulting impedance matrix to predict the currents frequency spectra. For validation, the currents are also measured. A measured current spectrum and a calculated current spectrum are both plotted in figure 5 in order to easily compare them.

As can be seen in figure 5 the calculated and the

measured spectra superimpose up to 110 MHz. The current spectrum prediction is valid up to 110 MHz, and the resulting matrix perfectly reflects the behavior of the output passive circuit.

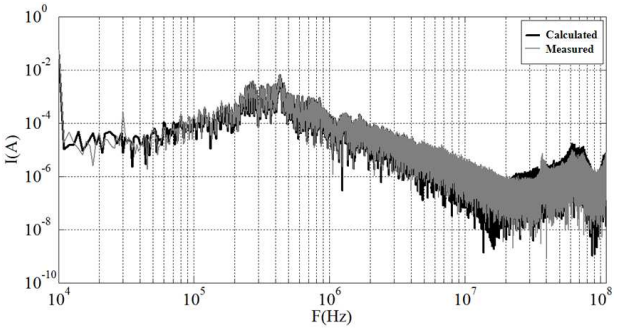

Fig.5. Blocks modeling by impedance matrices

IV. EXPERIMENTAL VALIDATION

The present approach uses the impedance matrices to predict and study the EMIs before assembling the pre-constructed parts of the system. The electronic systems are decomposed into blocks. Each passive part of the system is modeled by an impedance matrix which includes all its imperfections. Hereafter these matrixes can be then cascaded in order to rebuild the system in simple 2x2 matrix. Furthermore, using the resulting matrix and the input voltages, the flowing current frequency spectrum can be predicted. This method allows system integrators to isolate the different parts of the system into blocks, and then explore different placement and parts combinations for better electromagnetic compatibility. The current prediction is validated up to 110 MHz. It is important to note that in this paper this approach is applied on an integrated class D audio amplifier system, but could also be applied on any circuit with two active conductors and a ground conductor.

The future work will be focused on the class D output voltages prediction. Furthermore, this approach will be generated to be applied on power electronic systems with 3 active conductors and N active conductors.

REFERENCES

[1] R. Mrad, F. Morel, G. Pillonnet, C. Vollaire, D. Labrousse, *Differential passive circuit modelling with pentapole impedance matrices,* EMC Europe 2011, York, England.

[2] R. Mrad, F. Morel, G. Pillonnet, C. Vollaire, A. Nagari, *Conducted EMI prediction for integrated class D audio amplifier,* 18th international conference, ICECS 2011, Beirut, Lebanon

[3] R. Mrad, F. Morel, G. Pillonnet, C. Vollaire, P. Lombard, A. Nagari, *Approche de modélisation des chemins de propagation des perturbations conduites pour des systèmes à deux conducteurs actif,* CEM 2012, Rouen, France

[4] G. Pillonnet, R. Cellier, N. Abouchi, A. Nagari, *A High Performance Switching Audio Amplifier Using Sliding Mode Control,* IEEE Circuit and Systems and TAISA conference, pp. 305-309, 2008

[5] Micro Speaker http://www.seltech-international.com/index.php?/en/Products/NXP/Speakers/NXPSpeakers/65-RA9.6x13.6x2.9.html [Revised May 24, 2011].

Approche de Modélisation des Chemins de Propagation des Perturbations Conduites pour des Systèmes à Deux Conducteurs Actifs

Roberto Mrad[1,2,3], Florent Morel[1], Gaël Pillonnet[2], Christian Vollaire[3], Philippe Lombard[2], Angelo Nagari[3]

[1]Université de Lyon, ECL Ampère, UMR 5005
[2]Université de Lyon, CPE INL, UMR 5270
[3]ST-Ericsson, Grenoble, AMS BU

Résumé : La méthode de modélisation présentée dans cet article permet de prédire les spectres de courants d'un système électronique différentiel. Le système électronique considéré est décomposé en circuits élémentaires modélisés par des matrices d'impédances. L'association de ces blocs élémentaires permet de reconstruire le système. Ceci permet alors d'étudier l'impact fonctionnel de chacun des blocs et son influence CEM dans un système global. De plus l'assemblage des blocs permet l'obtention d'un modèle système compact pour des simulations CEM ultérieures.

Mots-clés : modélisation fréquentielle, matrice d'impédances, système différentiel.

1. INTRODUCTION

Dans cet article les matrices d'impédances ont été utilisées pour la modélisation des chemins de perturbations électromagnétiques conduites. Le but principal de cette approche est la prédiction des courants pour l'étude des perturbations électromagnétiques (EM) conduites avant l'assemblage des différentes parties d'un système. Dans des travaux antérieurs [1] seulement le mode commun à été abordé pour un système d'électronique de puissance et les matrices d'impédances ont été seulement déterminé par mesure à l'analyseur d'impédance. La présente méthode prend en compte le mode différentiel et le transfert de mode. Les matrices d'impédances sont déterminées par simulation et mesure à l'analyseur d'impédance ou à l'analyseur vectoriel. Cette méthode est destinée aux concepteurs et aux intégrateurs de systèmes électroniques afin d'étudier la compatibilité électromagnétique (CEM) en amont de la réalisation des prototypes.

La méthode proposée a été validée en l'appliquant sur une chaîne d'amplification audio pour des applications de téléphonie mobile contenant un amplificateur de type Classe D. Ces amplificateurs commutés ont un rendement élevé c'est pourquoi ils sont couramment utilisés dans des systèmes embarqués [2-3]. Cependant les amplificateurs de Class D commutent des courants qui peuvent atteindre un ampère avec des fréquences de commutation allant de quelques centaines de kilohertz jusqu'à quelques mégahertz, avec des temps de montée et de descente inférieurs à une dizaine de nanosecondes, ainsi ces circuits sont de fortes sources de perturbations. C'est pourquoi leurs émissions électromagnétiques doivent être étudiées pour limiter leur impact dans les systèmes fortement intégrés. Pour cela, les concepteurs essayent de trouver des méthodes de commande plus appropriées pour réduire leurs émissions. Bien souvent ces méthodes restent insuffisantes et des filtres CEM doivent être ajoutés. Cependant, la conception d'un filtre CEM n'est pas triviale [4] Ils ont souvent des réponses inattendues après construction et surtout lorsqu'ils sont associés avec d'autres circuits comme les charges. Dans le cas où les degrés de liberté sont seulement les circuits passifs, la présente méthode permet d'anticiper les problèmes pour faciliter le travail des intégrateurs.

La deuxième partie explique le principe de la méthode pentapolaire et décrit ses avantages. La troisième partie d'écris les applications pratiques sur un système d'amplification de Class D. Enfin, la dernière partie résume et conclut l'article.

2. METHODE PENTAPOLAIRE

La méthode pentapolaire consiste à décomposer un système électronique comportant deux conducteurs actifs et une masse en circuits élémentaires nommés blocs. La figure 1 montre la décomposition en blocs d'un système d'amplification audio où chacun des blocs est modélisé par une matrice d'impédances. Ensuite les différents blocs du système sont associés

pour reconstruire le système en une seule matrice modélisant le comportement de tous les blocs. Les parties passives étant modélisées alors par une seule matrice d'impédances, les tensions à leur entrée sont utilisées pour calculer les spectres des courants circulant dans le système. Ainsi, le comportement CEM du système et de chaque bloc dans le système peut être étudié.

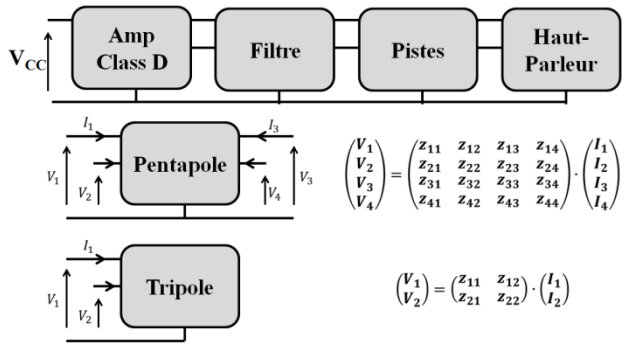

Figure 1: Décomposition en blocs du système d'amplification et représentation des blocs

Deux types de blocs peuvent être distingués. Les pentapoles modélisés par des matrices d'impédances 4x4 (deux entrées, deux sorties et une référence). Ces blocs se situent au milieu de la chaine et peuvent être reliés des deux cotés. Enfin les blocs tripolaires (comme la charge) modélisés par des matrices d'impédances 2x2 se situent à la fin de la chaine et ils n'ont pas de sortie électrique accessible [5]. Ces matrices d'impédances peuvent être déterminées par plusieurs méthodes : à partir de mesures (à l'analyseur d'impédance ou à l'analyseur de réseaux), ou à partir de simulations. Il existe deux types d'association de blocs : l'association de deux blocs pentapolaires et l'association d'un bloc pentapolaire avec un autre tripolaire. Les méthodes permettant de réaliser ces associations ainsi que des résultats expérimentaux ont été présentés dans un article précédent [5].

La méthode pentapolaire permet donc de modéliser le comportement fréquentiel des systèmes passifs différentiels. Elle prend en compte les éléments parasites des composants et leurs couplages [5], ainsi que les impédances des pistes du PCB. Cette méthode modélise également les perturbations EM sans être obligé de différencier les modes commun et différentiel, ce qui permet de modéliser toutes les perturbations y compris le transfert de mode.

3. VALIDATION EXPERIMENTALE

Cette méthode a été appliquée à un amplificateur audio de Classe D différentiel utilisé pour des applications de téléphones portables. Deux blocs passifs sont branchés à sa sortie : un filtre CEM et un haut-parleur. L'amplificateur utilisé est un amplificateur Classe D à hystérésis. Il présente un étalement de spectre au niveau de la fréquence de commutation et ses harmoniques. En effet, la fréquence de commutation est dépendante du signal d'entrée. Plus l'amplitude du signal d'entrée est élevée plus le spectre de sortie est étalé [6].

Les matrices d'impédances des blocs passifs (filtre, et haut-parleur) sont déterminées par mesure à l'aide d'un analyseur d'impédance [7] et d'un analyseur vectoriel [8]. En utilisant un analyseur d'impédance, la détermination de cette matrice consiste à mesurer les éléments de la diagonale (Z_{ii}), puis de déterminer les éléments croisés (Z_{ij} ; $i \neq j$) à l'aide de l'équation (1).

$$Z_{ij} = \sqrt{Z_{jj} \cdot (Z_{ii} - Z_{ijCC})} \qquad (1)$$

Z_{ij} est l'impédance croisée entre le port i et j. Z_{ii} et Z_{jj} sont les impédances vues du port i et j respectivement. Z_{ijcc} est l'impédance vue de i quand j est en court-circuit.

Cependant, dans certains cas les imprécisions de mesure peuvent conduire à des résultats aberrants. Un exemple est donné dans la figure 2. Les impédances Z_{11} et Z_{12CC} (Z_{12cc} impédance mesurée du terminal 1 quand le terminal 2 est en court-circuit) qui sont nécessaires pour le calcul de Z_{12} du filtre se superposent sur une grande plage de fréquence. La différence est inférieure à la précision de l'analyseur d'impédance. Le résultat du calcul n'a donc pas de réalité physique sur cette plage de fréquences. Donc dans le cas du présent filtre, la matrice d'impédance ne peut pas être mesurée par l'analyseur d'impédance pour des raisons de précision. Pour cela, l'utilisation l'analyseur vectoriel à quatre ports a été envisagée comme une solution pour la détermination de la matrice d'impédance du filtre. Par la suite, la matrice de diffusion du filtre est mesurée à l'aide de l'analyseur vectoriel. Puis, la matrice $[S]$ est transformée en matrice $[Z]$ en utilisant l'équation (2).

$$Z = (I - S)^{-1} \cdot (I + S) \cdot Z_0 \qquad (2)$$

S et Z sont les matrices de diffusion et d'impédances respectivement du bloc considéré. I est une matrice identité. Z_0 est l'impédance caractéristique de l'appareil et des câbles de mesure.

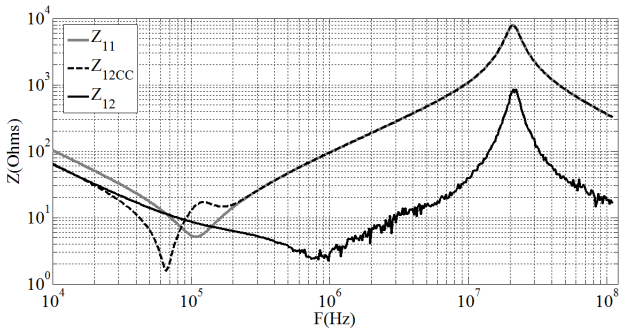

Figure 2:Analyse pour impédance croisée

Néanmoins, les paramètres *S* d'un bloc peuvent atteindre des niveaux inférieurs à la précision de l'appareil de mesure, ce qui mène à une imprécision dans les impédances calculées comme dans la figure 3. De plus, la précision des impédances peut varier entre impédance de diagonale (Z_{ii}) ou celle croisée (Z_{ij} ; $i \neq j$), et aussi suivant la valeur mesurée [9].

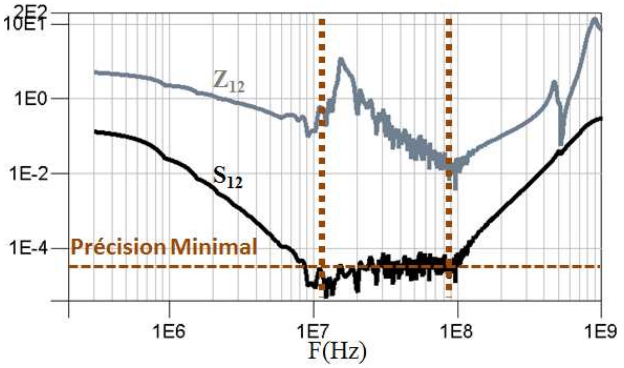

(a): Z_{12} & S_{12}

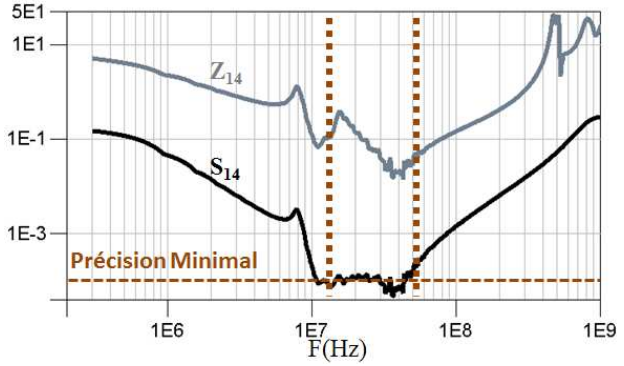

(b): Z_{14} & S_{14}

Figure 3:Impédance calculées à partir des paramètres S

Les simulations peuvent être finalement la solution pour remédier à la limitation des appareils de mesure. Pour cela, le logiciel ADS a été utilisé pour extraire la matrice de diffusion ou d'impédances du filtre (dans le cas de la matrice de diffusion, la matrice d'impédance est calculée à l'aide de l'équation (2)). Ce type de simulation permet d'introduire des composants de la librairie (qui ont un comportement proche de la réalité), ainsi que les impédances des pistes du PCB tout en prenant en compte les caractéristiques de la carte et du routage (épaisseur du substrat, largeur des pistes, architecture physique du PCB…). Cependant, la simulation présente aussi ses inconvénients. Le couplage des pistes entre elles, des composants entre eux et entre pistes et composants ne peut pas être pris en compte. Cela est dépendant de la forme du routage, du placement des composants les uns par rapport aux autres [10] et des technologies de fabrication de chaque composant. Pour cela ces phénomènes seront négligés dans ces simulations. La figure 4 montre une image de la simulation ADS du filtre. La figure 5 montre la comparaison des paramètres S du filtre mesurés à l'aide d'un analyseur vectoriel et simulés à l'aide d'ADS. La figure 6 montre la comparaison des impédances du filtre issues des trois méthodes de détermination déjà présentées (mesure à l'aide des l'analyseur d'impédance et vectoriel et simulation à l'aide d'ADS).

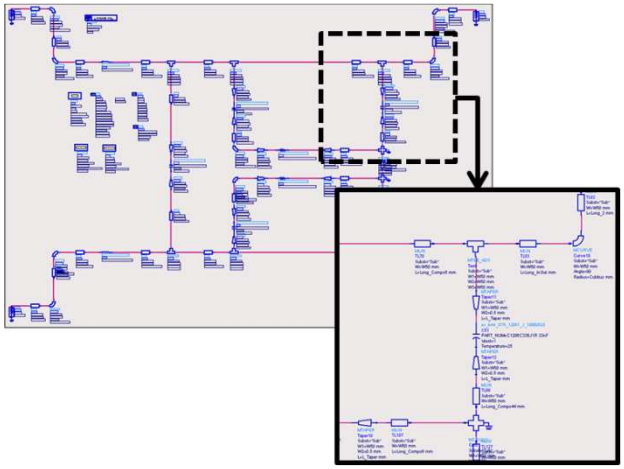

Figure 4 : Modèle ADS du filtre utilisé

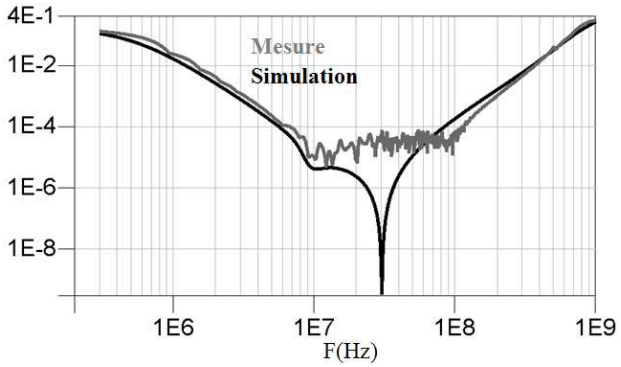

(a) Amplitude de S_{12}

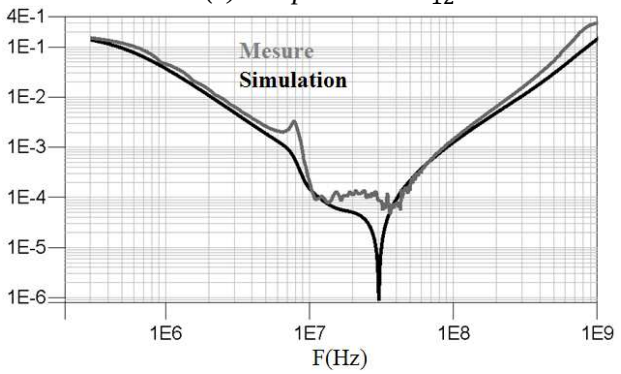

(b) Amplitude de S_{14}

Figure 5 : Paramètres S mesurés à l'aide d'un analyseur vectoriel et simulés à l'aide d'ADS

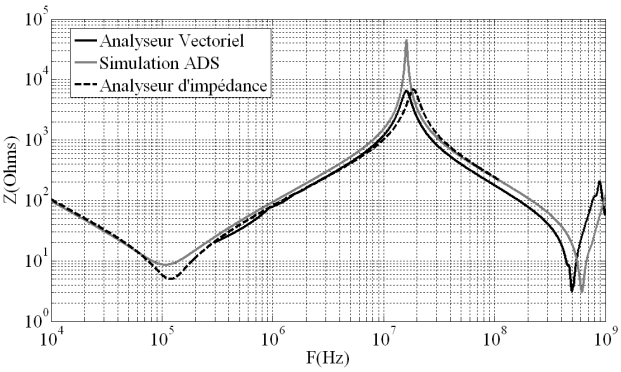

(a) Amplitude de Z_{12}

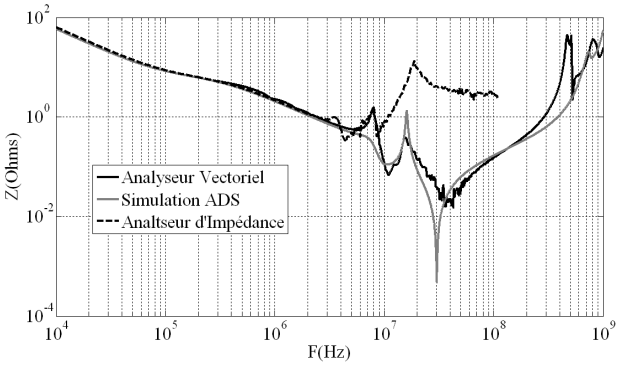

(b) Amplitude de Z_{14}

Figure 6 : Comparaison des trois types impédances

La figure 5 montre d'une part que les simulations du filtre à l'aide d'ADS concordent avec les mesures en paramètres S sur l'analyseur vectoriel. D'autre part cette figure montre la limitation de l'appareil sur les zones d'antirésonances, où les grandeurs mesurées sont inférieures à sa précision minimale. La figure 6 montre que les impédances issues des trois types de détermination concordent jusqu'à 2 MHz. Après cette fréquence les mesures à l'analyseur d'impédance divergent dans le cas des impédances croisées à cause des problèmes déjà évoqués, alors que les deux autres types concordent.

La prédiction des courants de sortie de l'amplificateur Classe D nécessite la connaissance des tensions de sortie. Les tensions de sortie peuvent être à leur tour déterminées par simulation ou par mesure (dans ce papier seule la mesure des tensions est traitée). Les tensions de sortie de l'amplificateur Classe D ont été mesurées avec des charges différentes (charge infinie, haut-parleur et haut-parleur avec filtre CEM), leurs spectres sont montrés dans la figure 7. La mesure des tensions à vide de l'amplificateur Classe D a été utilisée pour la prédiction des courants en prenant l'hypothèse suivante : les tensions de sortie de l'amplificateur Classe D utilisé sont très peu dépendantes des circuits passifs mis en aval, mais fortement dépendantes de la modulation (entrée audio). Cette hypothèse est justifiée par le fait que l'amplificateur comporte une contre réaction interne : le contrôleur agit de manière à ce que la tension de sortie suive la consigne indépendamment de la charge. Dans le cas où cette hypothèse n'est pas valable, un modèle équivalent de l'amplificateur est nécessaire [11-12]. Les tensions à vide mesurées (à l'aide de l'oscilloscope 12 bits [13] pour augmenter la précision de la quantification [14]) à la sortie de l'amplificateur et la matrice d'impédance résultante, permettent de calculer en utilisant la loi d'Ohm généralisée (3), les spectres de courants.

$$\begin{pmatrix} I_1 \\ I_2 \end{pmatrix} = Z_R^{-1} \cdot \begin{pmatrix} V_1 \\ V_2 \end{pmatrix} \qquad (3)$$

I_1 et I_2 sont les courants à calculer. V_1 et V_2 sont les tensions mesurées (dans le cas présent les tensions et les courants sont ceux de la sortie de l'étage de puissance de l'amplificateur de Classe D). Z_R est la matrice d'impédances 2×2 résultante après avoir associé tous les blocs du système.

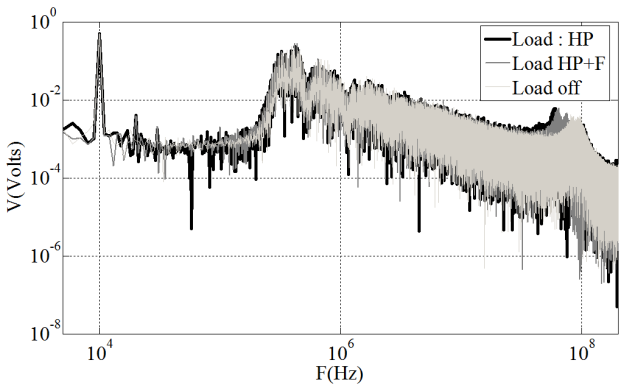

Figure 7:Tensions à la sortie de l'amplificateur avec différent types de charges

La méthode de calcul est montrée sur le schéma de la figure 8. La figure 9 montre la comparaison du spectre de courant mesuré (sonde de courant [15]) avec celui qui a été calculé, où la partie (a) montre les courants calculés en utilisant les matrices d'impédances issues de l'analyseur vectoriel (mesure de la matrice S puis transformation en matrice d'impédances à l'aide de l'équation (2)) et la partie (b) montre les courants calculés en utilisant les matrices d'impédances issues des simulations ADS.

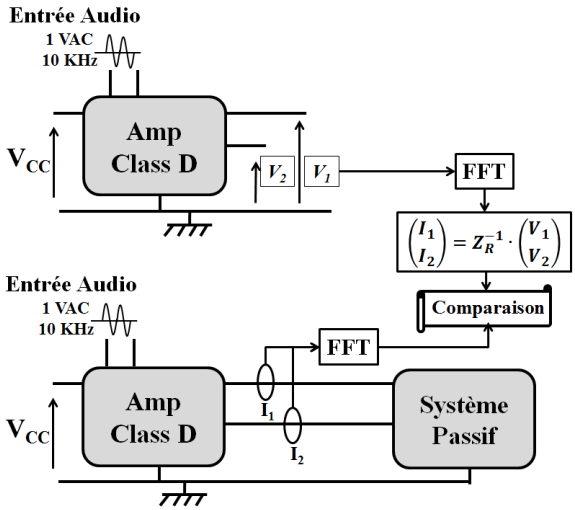

Figure 8:Procédure de calcul des spectres de courant

Comme il est montré dans la figure 8 les tensions sont mesurées en temporel pour avoir le déphasage relatif entre les voies 1 (V_1) et 2 (V_2) après la FFT. La figure 9 montre que le courant calculé est correct jusqu'à 110 MHz. Les courants concordent avec ceux mesurés dans le cas des matrices d'impédances mesurées à l'aide d'un analyseur vectoriel (Fig.9.a) ou simulés à l'aide d'ADS (Fig.9.b). Les spectres ne sont pas montrés au-dessus de 110 MHz car ils présentent des phénomènes de repliement de spectre.

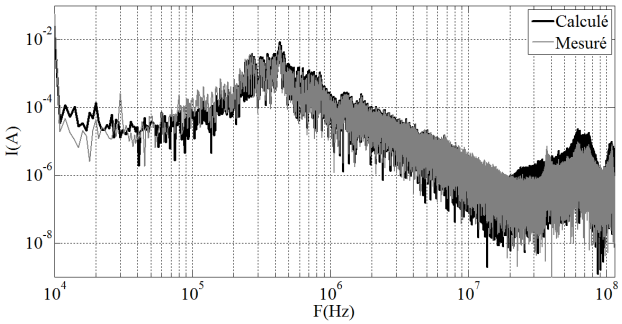

(a) : Courants calculés avec les matrices d'impédances mesurées avec un analyseur vectoriel

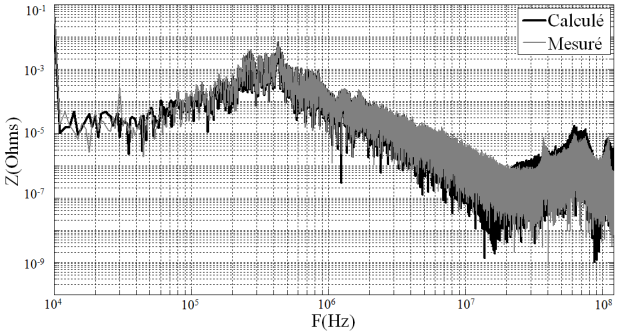

(b) : Courants calculés avec les matrices d'impédances simulées avec ADS

Figure 9: Comparaison du courant calculé avec le courant mesuré

4. CONCLUSION

Les matrices d'impédances des différents blocs du système ont été mesurées avec un analyseur d'impédance et un analyseur vectoriel, et aussi simulées à l'aide du logiciel ADS de Agilent (chaque méthode a un domaine de validité différent). Ces matrices ont permis d'avoir un modèle fréquentiel compact du système. Ensuite, en se basant sur l'hypothèse que la source de tension est idéale, les tensions à vide sont utilisées pour prédire les courants d'un amplificateur audio de type Classe D. La prédiction en courant a été testée jusqu'à la fréquence de 110 MHz. Ce qui a démontré les avantages et la précision de cette méthode.

Les intégrateurs de systèmes électroniques pourront bénéficier des avantages de cette méthode afin d'estimer les spectres de courant et donc la signature CEM dès la phase de conception. De plus, en utilisant la simulation pour la détermination des matrices d'impédances, cette méthode peut être un

outil de liaison entre la conception et l'étude CEM des systèmes. Cet outil est utile pour la conception de filtres et de routages afin d'améliorer la réponse CEM. Enfin, la méthode présentée requière un faible temps de simulation en comparaison des simulations temporelles. Les problèmes de CEM peuvent être donc localisés et traités au niveau de chaque bloc. Les intégrateurs de systèmes électroniques peuvent alors exploiter une meilleure combinaison de blocs passifs pour réduire les émissions d'un convertisseur différentiel donné. A titre d'exemple, plusieurs topologies de filtres CEM peuvent être rapidement étudiées dans un système global, en remplacent simplement le bloc fonctionnel par la matrice d'impédances correspondante. Ce principe peut être étendu à n'importe quel autre bloc élémentaire. L'accès ou la création de librairie permettra d'étendre les possibilités d'étude afin de faire les choix les plus judicieux dès la phase de conception.

5. REFERENCES

[1] C. Jettanasen, F. Costa, C. Vollaire, "Common-Mode Emissions Measurements and Simulation in Variable-Speed Drive System", *Power Electronics, Transaction on, Vol.24, pp. 2456-2464, November 2009.*

[2] International Rectifier, "Application note 1071, Class D Amplifier Basics".

[3] M. Berkhout, "Integrated Class Amplifier", *Convention Paper 5502, 112th Convention, Munich, Germany, Mai 2002.*

[4] R. L. Ozenbaugh, T. M. Pullen, "*EMI Filter Design, Third Edition*", Chapitre 1, Septembre 2011

[5] R. Mrad, F. Morel, G. Pillonnet, C. Vollaire et D. Labrousse, "Differential Passive Circuit Modelling With Pentapole Impedance Matrices", *EMC Europe 2011, York.*

[6] G. Pillonnet, N. Abouchi, R. Cellier, A. Nagari, "A 0.01% THD, 70dB PSRR Single Ended Class D using variable hysteresis control for headphone amplifiers", *Circuit and Systems, ISCAS 2009, IEEE International Symposium on.*

[7] Agilent, "*Precision Impedance Analyzer, Agilent 4294A*".

[8] Agilent, "*ENA RF Network Analyzer, Agilent 5071B*".

[9] Agilent, "*Application note 1369-2, Advanced impedance measurement capability of the RF I-V method compared to the network analysis method*", Tech. Rep., 2001

[10] S. Zangui, B. Vincent, K. Berger, R. Perrussel, E. Clavel, C. Vollaire, O. Chadebec, "Near-field coupling between EMC filter components", *14th Biennial IEEE, CEFC, Chicago, USA, 2010.*

[11] I.S. Steivano, I.A. Maio, F.G. Canavero, C. Siviero, "Parametric macromodels of differential drivers and receivers", *Advanced Packaging, IEEE Transactions on, May 2005.*

[12] D. Labrousse, B. Revol et F. Costa, "Switching cell EMC behavioral modeling by transfert function", *EMC Europe 2011, York.*

[13] Lecroy, "*Lecroy WaveRunner 6 Zi Digital Oscilloscope* ".

[14] R. Mrad, F. Morel, G. Pillonnet, C. Vollaire, A. Nagari, "*Conducted EMI Prediction for Integrated Class D Audio Amplifier*", 18th International Conference, ICECS, Beirut, Lebanon, 2011.

[15] Tektronix, "*Tektronix P6022 Current Probe*".

Contribution To A Methodology Of Mechatronic System Design : MODEL INVERSION AND UNCERTAINTY PROCESSING

Van Hoa Nguyen

Wilfrid Marquis-Favre, Damien Eberard, Project: OPENPROD, Ampère Lab

***Abstract*— This thesis aims to provide a systematic method for uncertainty processing in mechatronic systems design and furthermore, for tolerance synthesis.**

The problem of system design, in general, and/or the problem of sizing, in particular, aims to response the question: What system/component do we have to choose to satisfy the given specifications. For example, in a hoist engine, we desire to move the masse with a certain velocity, what motor do we have to use, and how should we adjust its parameters? In engineering, the system design problem is considered in the V cycle, which consists of 2 phases: from the client's specifications to the virtual prototype and from the virtual prototype to the production of real system.

In the process of system design, there are always uncertainties and imprecisions in the specifications and measures. Moreover, the produced components are usually not exactly the desired value, due to variations in the fabrication process. As consequence, we need to take into consideration the uncertainties, both in design process and in fabrication process, in order to improve the performance and robustness of system.

***Résumé*—**

I. CONTEXT AND PROBLEMATIC OF THE THESIS:

A. Context:

This thesis takes part in the European project ITEA2 OPENPROD: "Open model driven whole-product Development and simulation environment". The project is composed of 27 partners (laboratories and industrial companies) from 5 countries (France, Germany, Sweden, Switzerland and Finland). The project aims to develop an environment for modeling and simulation, which integrates Eclipse with the open-source tools of OpenModelica.

This thesis is in the theory study part of the project. Its works concern the mechatronic systems design with consideration of uncertainties.

B. Problematic:

The problem of system design, in general, and/or the problem of sizing, in particular, aims to response the question: What system/component do we have to choose to satisfy the given specifications. For example, in a hoist engine, we desire to move the masse with a certain velocity, what motor do we have to use, and how should we adjust its parameters?

In engineering, the system design problem is considered in the V cycle, which consists of 2 phases: from the client's specifications to the virtual prototype and from the virtual prototype to the production of real system.

In Ampère laboratory, a design methodology based on model inversion has been being developed for about 15 years. This methodology has proven its interest, compared with the direct method, in term of design time and real system performance.

In the process of system design, there are always uncertainties and imprecisions in the specifications and measures. Moreover, the produced components are usually not exactly the desired value, due to variations in the fabrication process. As consequence, we need to take into consideration the uncertainties, both in design process and in fabrication process, in

order to improve the performance and robustness of system.

This thesis aims to provide a systematic method for uncertainty processing in mechatronic systems design and furthermore, for tolerance synthesis.

II. Approach taken and justification from the literature:

A. For modeling: Bond graph

Justification: Bond graph is a multidiscipline language for modeling. Based on the concept of effort and flux, it can model an entire mechatronic system, which consists of several physic domains, in only 1 graph. The tools for model structure analysis and model inversion are already available in the works of JARDIN and EL FEKI.

For sizing: The system design methodology based on model inversion.

Justification: The methodology based on model inversion has proven its interest, compared to the direct method (try – error - correction), both in term of design time and real system performance. The criteria of inversibility and inversion procedures are well developed in the work of NGWOMPO and JARDIN, as well as some others in Ampère laboratory.

B. For uncertainty processing: Probability theory and fuzzy logic.

Justification: Uncertainties in a mechatronic system are classified into 2 classes: aleatory uncertainty, which is associated to the variability of a size, and epistemic uncertainty associated to the ignorance on a size. These 2 types of uncertainty have their respected tools for processing. The fuzzy logic considers the satisfaction level of a system performance, with respect to the desired performance. On the other hand, the probability theory treats the variability of real value of components in the fabrication, and hence the quality of production process. The result of fuzzy logic approach is used in quality control of a unit while the result on probability approach is used for the industrial massive production. These 2 approaches are therefore complementary and can be combined for a systematic process of uncertainty treatment in mechatronic system.

III. The work actualized:

- Research on the uncertainty processing in a mechatronic system design, using model inversion, probability theory and fuzzy logic.
- Proposition a designing methodology with consideration of uncertainty, which is attached to the V design cycle.
- The proposed methodology is applied on an example of sizing a continuous courant motor.
- The methodology is based on both probability theory and fuzzy logic, in the aim for a complete uncertainty processing in mechatronic system design. The comportment of system is considered in stationary state and dynamic regime, to consider also the system performance and constraint in transitive regime.
- The obtained result is not always ready for production (for example, not in the form of a normal law, which is demanded by the manufacturer, or there is a constraint to respect…). Therefore, we proposed an adaptation phase in order to modify the obtained result, for production.
- The result of probabilistic approach is used to determine the fabrication tolerance, whereas the result of fuzzy logic approach is used for system performance evaluation.
- Participating and presenting the research results at the meeting/seminars of project OPENPROD and group SEEDS.

IV. Conclusion and outlook:

A. Conclusion:

- The work of this thesis has taken into account the uncertainty in the methodology of mechatronic system design.
- The interest of designing by model inversion and the adaptation phase is proven.

B. Outlook:

- Formulation of the adaptation method, using a combination of probability theory and fuzzy logic
- Considering the results of multi variables case. We are also heading for an aleatory process
- Research for other mean of uncertainty propagation.

Diagnostic by New unsupervised methods

Abdenour. SOUALHI
Hubert. RAZIK, Guy. CLERC
Laboratoire AMPERE, CNRS, UMR5005, Bât. Oméga,
43 bd du 11 novembre 1918, Villeurbanne, 69622
E-mail : [abdenour.soualhi, guy.clerc, hubert.razik]@univ-lyon1.fr

***Abstract*— When we use a classifier in the field of condition monitoring, it is very common to be confronted with missing or unlabeled data. This lack of information constitutes a problem in the detection and diagnosis of faults because the classification quality of any monitoring system is defined by the quality of data used in the input of the classifier process.**

This phenomenon occurs when the measurements have not been labled or observed, they were lost or have not been recorded. The presence of these latter cause a malfunction of the monitoring system, since the classifier can not learn from incomplete databases. To correct this drawback, we adopt an alternative approach based on unsupurvised classification of data. The development of new methods based on unsepervised classification provide an attractive alternative to solve the problem of missing data and, subsequently, generate models for diagnosis and prognosis.

***Résumé*— Lors de l'utilisation d'un classificateur dans le domaine de la maintenance conditionnelle, il est très fréquent d'être confronté à des données non étiquetées ou manquantes. Ce manque d'information constitue un problème lors de la détection et le diagnostic des défauts, car la qualité de classification de n'importe quel système de surveillance est définie par la qualité des données utilisées dans le processus de traitement c'est à dire. à l'entrée du système de surveillance.**

Ce phénomène se manifeste lorsque les mesures n'ont pas pu être étiquetées ou observées, qu'elles ont été perdues ou qu'elles n'ont pas été enregistrées. La présence de ces dernières entraîne un dysfonctionnement du système de surveillance, puisque le classificateur, ne peut pas apprendre à partir des bases de données incomplètes. Si l'on veut l'utiliser, il faut donc adopter une autre approche que la classification supervisée sur ces données. L'élaboration de nouvelles méthodes basées sur la classification non supervisée s'avèrent une alternative très intéressante pour résoudre le problème de données manquantes et, par la suite, générer des modèles pour le diagnostic et le pronostic.

I. INTRODUCTION

Condition monitoring is based on two strategies: the first one is based on a model of the system under study. It represents the normal behavior of the system in the case of absence of faults. This model is used to generate residuals which indicate changes between the model and the fault affecting the system. However, it is necessary to have a complete and accurate model taking into account disturbances and errors due to unknown dynamics which are, unfortunately filtered by the model. The second one is based on signal processing. Signals may be studied either by using time-domain methods including correlation, mean-change, or using frequency-domain methods like spectral analysis, or with more sophisticated methods including time–frequency or wavelet analysis.

The aim of my PhD is to introduce new approaches for condition monitoring based on signal processing. These approaches use pattern recognition (PR) technique to detect several operating mode, in particular, the simultaneous occurrence of multiple faults. Pattern recognition is based on the extraction of information through the processing of measured signals like (currents, voltages, speed, vibration, temperature, noise ...) which can provide significant information about the defects. From these features, the implementation of classification methods (artificial ant system, hidden Markov models, neuro-fuzzy systems) allow the design of monitoring systems or algorithms performing the diagnosis and prognosis. The performances of these methods are closely related to the relevance of fault indicators selected.

The applications of pattern recognition include document classification, bioinformatics, data mining, speech recognition and industrial automation. In the following, Ω_1, Ω_2, ..., Ω_M will be the M different

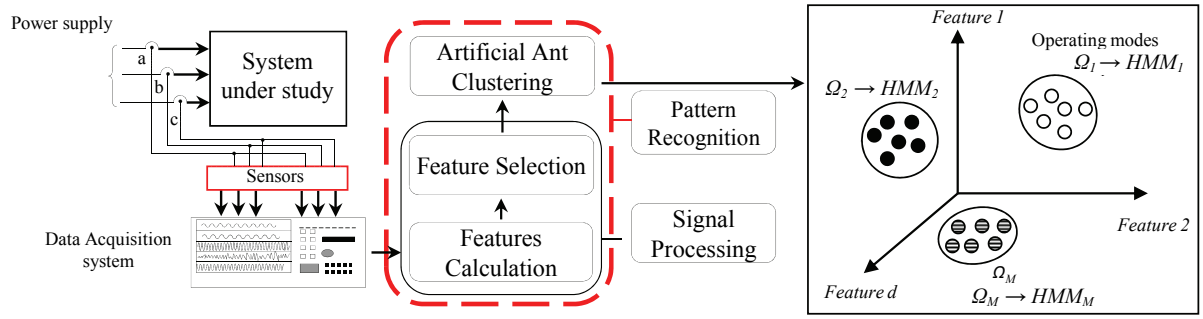

Fig.1 . Condition monitoring based on signal processing and pattern recognition.

classes of a pattern recognition problem. An object x_i is characterized by d-dimensional feature vector $x_i=(x_1,..x_j...x_d)^T$. The objective is then, given a pattern x_i, to decide if it should be assigned to the Class Ω_1 or Ω_2, ..., or Ω_M. Each class has a geometric area of d-dimensional space. Solving a problem of pattern recognition finally comes down to separate the different classes and define the boundaries separating them.

The technique described above, can be applied to the monitoring of a complex systems. In this case, the d-parameters of the feature vector result of measurements performed on the system to monitor. A good knowledge of the system can help us to choose the most appropriate features. These features, once chosen, are measured continuously on the system being monitored. Noise measurements and various disturbances can appear. The feature vector x, resulting from the same state of the system, will not find a single point, but an area of the d-dimensional space. If the features are well chosen, each operating mode can be represented by a class of the representation space as shown in Fig. 1.

II. FAULTS DETECTION AND DIAGNOSIS APPROACH

In the case of detection and diagnosis, the obtained classes represent the known and unknown operating modes. The detection and diagnosis consist in classify new measurements and then identify their assigned classes. Fault detection and diagnosis approach proposed in my PhD thesis is done in two stages: signal processing and classification. The pre-processing is used to find the necessary set of features to build the representation space, but some of them are redundant or not enough sensitive to faults. Then this number is reduced by the feature selection methods. The classification stage builds classes which characterize the different operating modes and affects new measurements into one of the predefined classes.

In the classification stage, we introduce a new optimization technique inspired by the behavior of real ants to improve the classification; it is an unsupervised technique designed to find the existing operating modes and the new ones in the database. The aim is to group a set of data into classes (Ω_1, Ω_2, ..., Ω_M) and affect new data into these classes such that similar data are placed in the same classes while dissimilar data are in separated classes. These classes are obtained by a similarity function which depends on the pheromones deposited by ants on the carried data and the distance separating these latter.

In the decision rule, we proposed the use of Hidden Markov models (HMMs) in order to assign the new measurements in the obtained classes. For this purpose we use the well-known Baum-Welch procedure to find the best HMM parameters λ (transition matrix A, observation matrix B and initial state vector π). This procedure is a variation of the more general EM algorithm, which iterates between two steps: the Expectation step and the Maximization step.

Given a series of T observations $O = (o_0,o_1,o_2,\ldots,o_T)$ extracted from the measurements and a HMM with complete parameters λ, the probability that this series was generated by the model is defined by $P(O|\lambda)$. The HMM, for which the probability is maximum, determines the health condition of the system (system in healthy, faulty mode). The architecture of the proposed approach is given in Fig. 2.

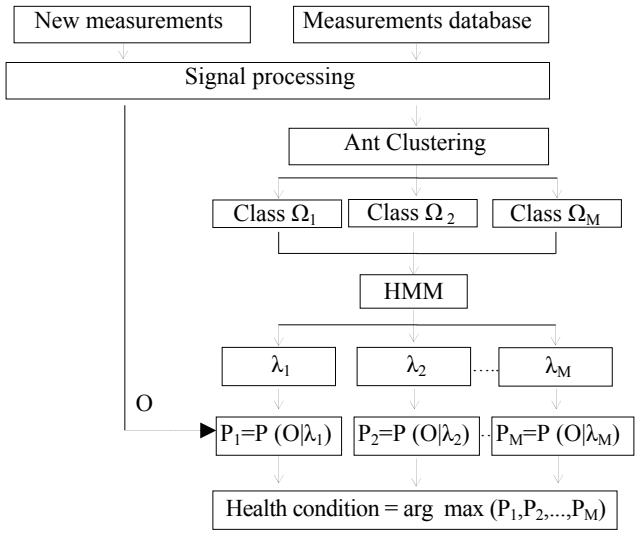

Fig. 2. Scheme of the proposed Fault Detection and Diagnosis approach.

III. PROGNOSIS APPROACH

Contrary to fault detection and diagnosis, these classes (obtained by the ant clustering technique) represent the ageing states of the system. The prognosis consists in predicting the future state of the system and estimating the remaining useful life. The aim of future state prediction is to estimate when the system is going to change from one state to another. It is impossible to predict the exact moment when a system is going to change states. However, it should be possible to give a reasonable estimation about when the system can be expected to go from one state to another. It is also possible to estimate a probability that indicates the chance that the system is going to change states in a certain amount of time. Future state prediction is done by estimating the state transition point to the final state. In this case we will assume that the final state transition is the one of interest since the system will be in need of repair once the final state transition point is detected. However, if the last state transition point is not the one of interest the proposed method can be used to estimate all future state transitions.

A weakness of the proposed state prediction method is that historical data about the system until failure needs to be recorded before a prediction can be made. This is because the prediction method needs some information from the system to determine the final state transition point.

Given an observation sequence $O = (o_0,o_1,o_2,\ldots,o_t)$ and hidden Markov models with complete parameters λ designed from the ageing states, the probability that the system is going to change states at time t+1 is given by $P(o_0,o_1,o_2,\ldots,o_t,o_{t+1} \mid \lambda)$. The HMM, for which the probability is maximum, determines the future state of the system. HMM-based fault prognosis architecture is given in Fig. 3.

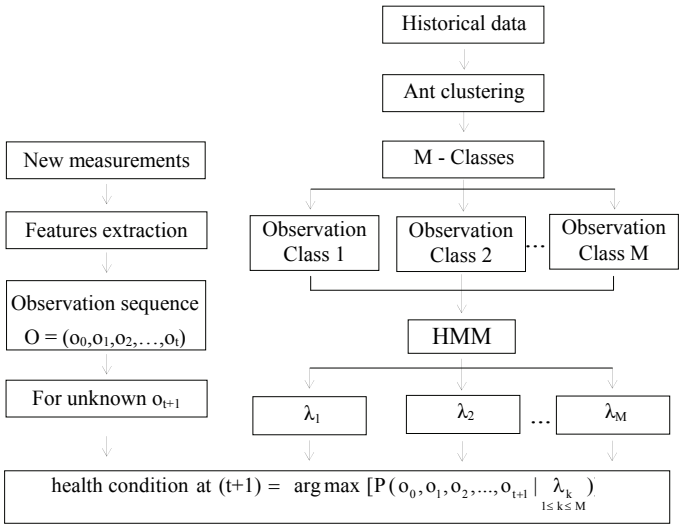

Fig. 3. Scheme of HMM-based Fault Prognosis.

IV. EXPERIMENTAL RESULTS

The proposed fault detection and diagnosis approach is validated in an asynchronous motor of 5.5 kW, 11.8A and 1440 rpm with 28 bars, 380V, 4 poles and 50 Hz as shown in figure 4.

Three voltage sensors and three current sensors were used. A powder brake has been used to simulate the shaft load; the motor is fed from three-phase inverter which makes more difficult the detection of the faulty modes. All measurements are made in steady state condition.

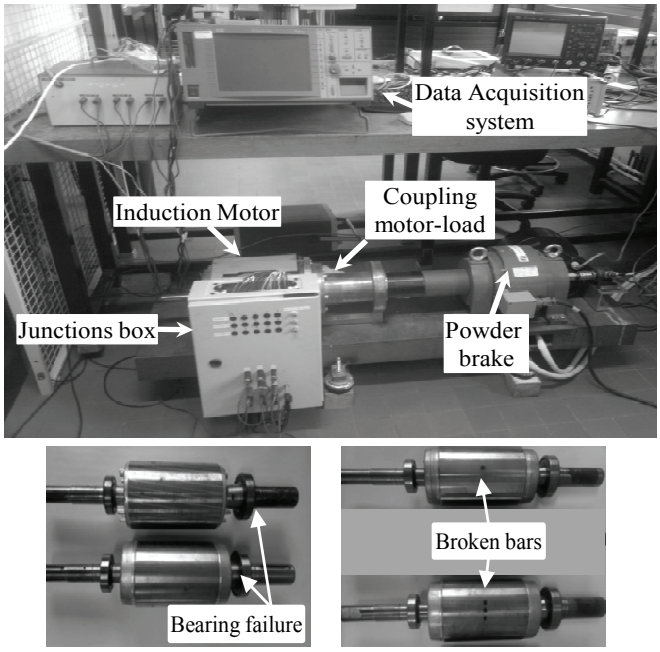

(a) Bearing failure (b) Broken bars

Fig. 4. The test-bed used for the monitoring.

The efficiency of the proposed approach is tested in three cases:

- *Complete knowledge in the operating modes.*
- *Unknown information on one of the operating modes;*
- *Incomplete knowledge in the operating modes.*

The proposed prognostic approach is validated by using real data of bearing defect degradation obtained from experimental work [1]. These data was generated by NSF I/UCR center intelligent Maintenance Systems (IMS) with support from Rexnord Corp.

The test bed is composed of four Rexnord ZA-2115 double row bearings installed on one shaft as shown in Fig. 5. These bearing have the following characteristics:

TABLE I: CHARACTERISTICS OF THE STUDIED BEARINGS

Roller diameter (in)	0.331
Number of Rollers/Row	16
Pitch diameter (in)	2.82
Contact Angle (deg)	15.17

The rotation speed was kept constantly at 2000 tr/min with 6000 lbs radial load placed onto the shaft and bearing by a spring mechanism. A PCB 353B33 High Sensitivity Quartz ICP Accelerometer was installed on the horizontal (X) and vertical axis (Y) for each bearing. The vibration data were recorded each 20 minutes with a fixed sampling rate of 20 kHz.

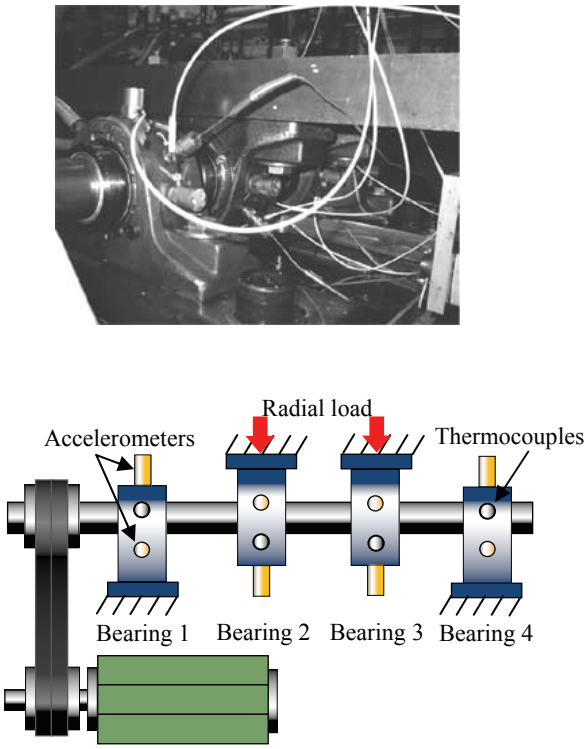

Fig. 5. Prognosis test bed [1]

V. CONCLUSION AND PERSPECTIVES

Currently several approaches have been proposed in my PhD to intelligent fault detection, diagnosis and prognosis based on signal processing and pattern recognition. In the design of the classifier, the ant clustering technique has been proposed as an unsupervised classification method inspired by the behaviour of real ants to optimize the detection of faults. The HMMs have been proposed as a decision rule for the assignment of new measurements to optimize the diagnosis of faults. They have been rigorously tested in different situations; the obtained results prove the efficiency of this approach for detection and diagnosis of broken bars and bearing failures at different load levels. In addition, the results obtained show that unlike the unsupervised ant clustering technique, the research of intelligent fault detection and diagnosis methods primarily dominated by supervised algorithm often fails when encountered by limited information in the operating modes for novel data for classification. Thus leading to lower acceptance of these methods especially in the industry, where obtaining labeled for different operating modes may be difficult.

The future state prediction approach presented in my PhD attempts to predict the future state of the system. The HMMs which are necessary for state transition prediction are created from the historical data about the system until failure. The prediction was tested on four double row bearings installed on one shaft. The current results confirm that the proposed approach is a good way to predict the future state of the system under study.

Then, the perspectives of my future works will focus on the estimation of the remaining useful life based on the specification of a neuro-fuzzy system that is able to reproduce (by approximation) the evolution of the properties of the system under study, and to predict a degradation state at any time. More precisely, developments aim at proposing an architecture that combines a neuro-fuzzy and a PI controller to satisfy an objective of prediction error control, whatever the horizon of prediction is.

PUBLICATION

- A.Soualhi, G. Clerc, and H. Razik, "Faults classification of induction machine using an improved ant clustering technique," in *Diagnostics for Electric Machines, Power Electronics Drives (SDEMPED), 2011 IEEE International Symposium on*, sept. 2011, pp. 316 –321.
- A.Soualhi, G. Clerc, H. Razik, and O. Ondel, "Detection of induction motor faults by an improved artificial ant clustering," in *IECON 2011 - 37th Annual Conference on IEEE Industrial Electronics Society*, nov. 2011, pp. 3446 –3451.
- A.Soualhi, G. Clerc, H. Razik, and A. LEBAROUD "Fault Detection and Diagnosis of Induction Motors Based on Hidden Markov Model," *ICEM 2012*.
- A.Soualhi, "Détection des défauts dans les moteurs asynchrones par une nouvelle méthode basée sur les fourmis artificielles," Conférence jeunes chercheurs en génie électrique, 13 décembre 2011.
- A.Soualhi, G. Clerc, H. Razik "Detection and Diagnosis of Faults in Induction Motor Using an Improved Ant Clustering Technique" submitted

REFERENCE

[1] NSF I/UCRC CENTER FOR INTELLIGENT MAINTENANCE SYSTEMS, "PROGNOSTIC DATA REPOSITORY: BEARING DATA SE,".